AD610943

Ok

RADC-TDR-64-481

# ACCELERATED TESTING OF HIGH RELIABILITY PARTS

COPY 2 OF 3 vmd
HARD COPY $. 3.00
MICROFICHE $. 0.75
95p

TECHNICAL DOCUMENTARY REPORT NO. RADC-TDR-64-481

January 1965

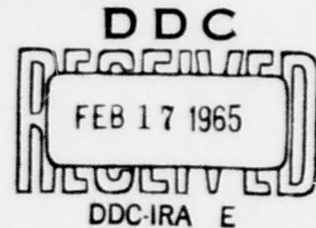


Reliability Branch

Rome Air Development Center
Research and Technology Division
Air Force Systems Command
Griffiss Air Force Base, New York

Project No. 5519, Task No. 551902

(Prepared under Contract AF 30(602)-3415 by General Electric Company, King of Prussia, Pennsylvania.)

ARCHIVE COPY

BLANK PAGE

When US Government drawings, specifications, or other data are used for any purpose other than a definitely related government procurement operation, the government thereby incurs no responsibility nor any obligation whatsoever; and the fact that the government may have formulated, furnished, or in any way supplied the said drawings, specifications, or other data is not to be regarded by implication or otherwise, as in any manner licensing the holder or any other person or corporation, or conveying any rights or permission to manufacture, use, or sell any patented invention that may in any way be related thereto.

Qualified requesters may obtain copies from Defense Documentation Center.

Defense Documentation Center release to Office of Technical Services is authorized.

Do not return this copy. Retain or destroy.

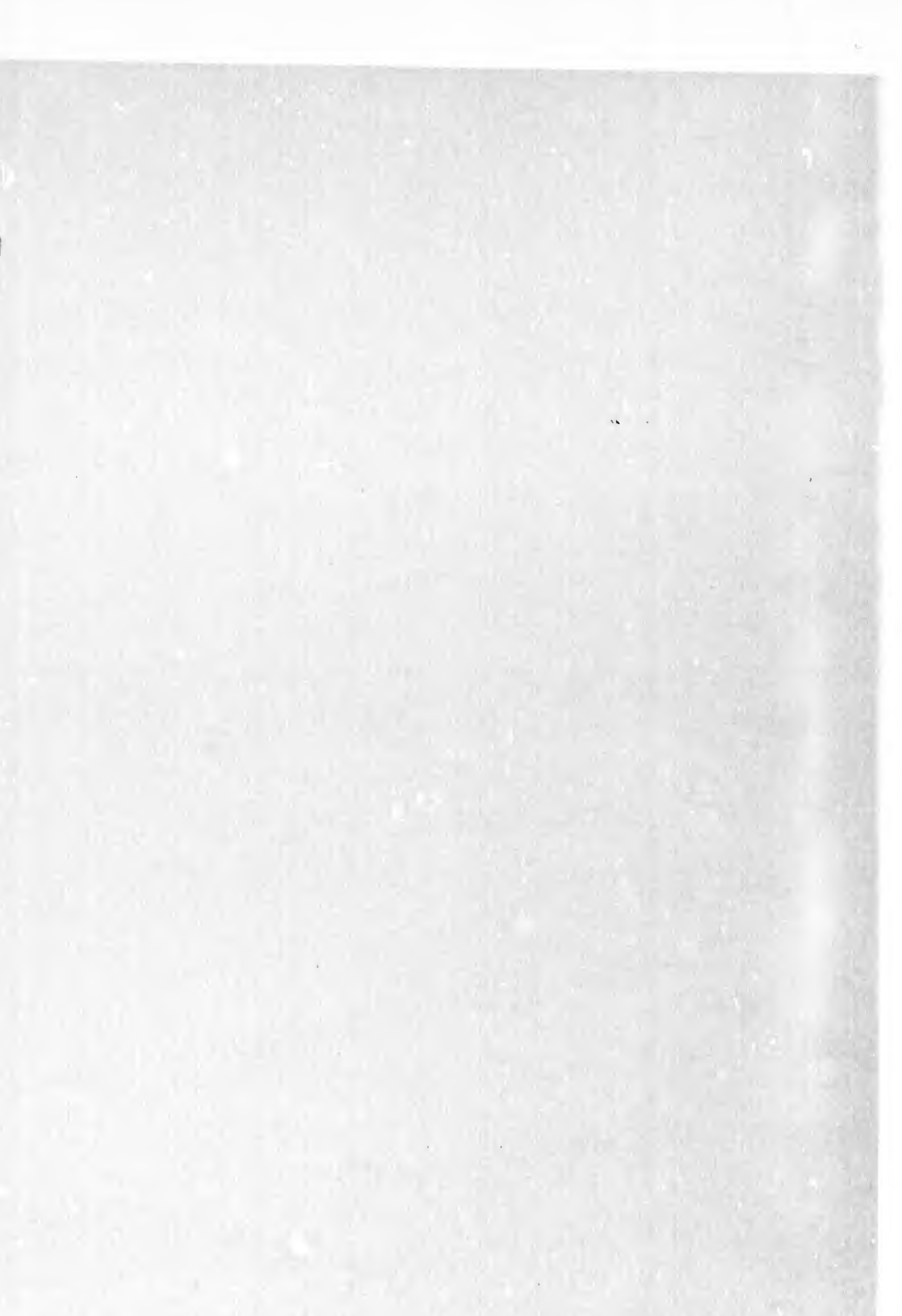

## FOREWORD

This report was prepared by the General Electric Company, on Contract AF30(602)-3415 under Task 551906 of Project No. 5519. This is the first Interim Technical Report describing the work performed for the period 10 June 1964 to 10 October 1964.

The report was written by T.M. Walsh, H.S. Endicott, G. Best, G. Bretts, H. Lampert and H. MacLean.

The work was performed at the Valley Forge Space Technology Center of the Spacecraft Department of General Electric Company, King of Prussia, Pennsylvania.

AIR FORCE, GAFB, N.Y., 16 FEB 65-129

## ABSTRACT

ACCELERATED TESTING OF HIGH RELIABILITY PARTS

A review of data and information gathered during previously conducted accelerated test programs has led to the formulation of degradation models for the parts under study. Long term constant stress tests, which were inactive for a 9 month period after accumulating 5000 to 9000 hours of test time at various stress conditions, were restarted. The effect of the passive period on the long term part parameter trends is discussed. Accelerated step stress test designs and analysis plans were formulated for metal film resistors and semiconductors and step-stress tests were initiated. Failure Mechanism Studies led to the formulation of a current conduction model for glass dielectric capacitors; the detection, possible source and estimated effects of phosphorous compounds on surface leakage of transistors; and low temperature characterization of diode surface leakage currents.

This is an interim report containing information on the first four months of Contract AF 30(602)-3415.


## PUBLICATION REVIEW

This report has been reviewed and is approved. For further technical information on this project, contact Mr. Mario L. Rocci, EMERR, Ext 6246

Approved: 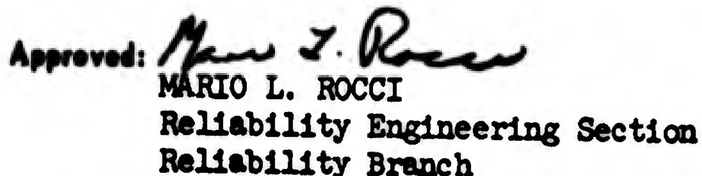
MARIO L. ROCCI
Reliability Engineering Section
Reliability Branch

Approved: 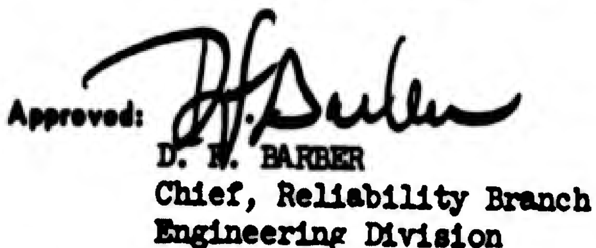
D. R. BARBER
Chief, Reliability Branch
Engineering Division

BLANK PAGE

## TABLE OF CONTENTS


| Section | | Page |
|---|---|---|
| 1 | INTRODUCTION | 1-1 |
| 2 | ACCELERATED TESTING TECHNIQUES | 2-1 |
| | 2.1 Introduction | 2-1 |
| | 2.2 Description of Test Program | 2-1 |
| | 2.2.1 General | 2-1 |
| | 2.2.2 Details of Test Program | 2-5 |
| | 2.3 General Analysis Approach | 2-6 |
| | 2.3.1 Deterioration of Part Parameter | 2-7 |
| | 2.3.2 Degradation of Ultimate Strength | 2-9 |
| | 2.4 Analysis Plan | 2-9 |
| | 2.4.1 Parts Where Deterioration can be Measured | 2-10 |
| | 2.4.2 Parts Whose Failure are Catastrophic | 2-12 |
| | 2.5 Relationship of Progressive Stress and Constant Stress | 2-14 |
| | 2.6 Relationship of Step Stress and Constant Stress | 2-16 |
| | 2.7 Analysis of Advent Test Data | 2-17 |
| | 2.7.1 Resistors | 2-17 |
| | 2.7.2 Capacitors | 2-26 |
| | 2.7.3 Semiconductors | 2-28 |
| 3 | FAILURE MECHANISM STUDIES | 3-1 |
| | 3.1 Resistors | 3-1 |
| | 3.1.1 Metal Film Resistors | 3-1 |
| | 3.1.2 Oxide Film Resistors | 3-6 |
| | 3.2 Capacitors | 3-9 |
| | 3.2.1 Glass Capacitor | 3-9 |
| | 3.3 Semiconductors | 3-17 |
| 4 | SPECIFICATION AND PROCUREMENT | 4-1 |
| | 4.1 General | 4-1 |
| | 4.2 R-Part Specifications | 4-1 |
| | 4.3 Quality Assurance Provisions | 4-2 |
| | 4.4 Discussion of Screening Tests | 4-3 |
| | 4.4.1 General | 4-3 |
| | 4.4.2 Specification Controls | 4-4 |
| | 4.4.3 Screening Tests | 4-4 |
| | 4.4.4 Parameter Drift Criteria | 4-6 |
| | 4.4.5 Screening Criteria | 4-6 |
| | 4.4.6 Linear Discriminants | 4-8 |

## TABLE OF CONTENTS (Continued)


| Section | | Page |
|---|---|---|
| 5 | SUMMARY AND CONCLUSIONS | 5-1 |
| 6 | WORK PLANNED FOR THE NEXT PERIOD | 6-1 |
| | 6.1 Resistors | 6-1 |
| | 6.2 Capacitors | 6-1 |
| | 6.3 Semiconductors | 6-1 |
| | 6.3.1 Surface Effects Investigation | 6-2 |
| | 6.3.2 Ohmic Contact Investigation | 6-2 |
| **Appendix** | | |
| I | Derivation of the $\theta$ Parameter | A-I-1 |
| II | Derivation of Model for Sodium Ions at Equilibrium with Field in Glass Capacitors | A-II-1 |
| III | Additional Development of the Expression for Calculating Electrostatic Potential and Electric Field at Ion Transport Equilibrium | A-III-1 |
| IV | Development of Numerical Values to be Used in Calculating Electrostatic Potential and Electric Field | A-IV-1 |
| V | The Ultraviolet Absorption Edge and Calculation of Forbidden Energy Gap | A-V-1 |
| VI | Equipment and Procedures Used in Measuring Capacitor Absorption and Leakage Current | A-VI-1 |
| VII | Diode Heat Transfer Study | A-VII-1 |

## LIST OF ILLUSTRATIONS


| Figure | | Page |
|---|---|---|
| 2-1 | General Test Plan | 2-3 |
| 2-2 | R2016P1003 -Phase I, II and III Damage Relationships | 2-22 |
| 2-3 | R2016P1003 - Design Life Data Chart | 2-23 |
| 2-4 | R2016P1003 - Phase IV - Resistance Variations | 2-25 |
| 2-5 | R2008P5 Failure Pattern | 2-29 |
| 2-6 | R2008P10 Design Data Chart | 2-29 |
| 2-7 | Leakage Current as a Function of Time | 2-31 |
| 3-1 | 10,000 Ohm Metal Film Resistor - Resistance Change | 3-3 |
| 3-2 | 20,000 Ohm Metal Film Resistor - Resistance Change | 3-4 |
| 3-3 | 100,000 Ohm Metal Film Resistor - Resistance Change | 3-5 |
| 3-4 | Absolute Resistance Change as a Function of Time-Temperature Parameter for 100,000 Ohm Metal Film Resistor | 3-7 |
| 3-5 | 100,000 Ohm Oxide Film Resistor - Resistance Change | 3-8 |
| 3-6 | Absolute Resistance Change as a Function of Time-Temperature Parameter for 100,000 Ohm Oxide Film Resistor | 3-10 |
| 3-7 | Glass Capacitor | 3-11 |
| 3-8 | Glass Capacitor Failure Distribution | 3-11 |
| 3-9 | Energy Bands and Ion Distribution | 3-14 |
| 3-10 | Leakage Current Versus Applied Voltages at 150°C | 3-16 |
| 3-11 | Leakage Current Versus Applied Voltages at 225°C | 3-16 |
| 3-12 | Inversion Layer Formation | 3-19 |
| VI-1 | Schematic Circuit for Long Time Current Measurements in R2045P151 Capacitors | A-VI-2 |
| VI-2 | Schematic Circuit for Short Time Current Measurement in R2045P151 Capacitor | A-VI-4 |

BLANK PAGE

# 1. INTRODUCTION

This report is the First Technical Documentary Report to be prepared under Contract AF30(602)-3415, Task 551906 and Project No. 5519.

The purpose of the program is to study, investigate, and develop the test and measurement techniques for controllable accelerating of electronic parts aging; and to perform an investigation, study and analysis of the failure mechanisms of the high reliability parts used. A listing of the high reliability parts which are being studied is shown in Table 1-1.

TABLE 1-1. DESCRIPTION OF PARTS ON TEST

| R NUMBER | DESCRIPTION | CLOSEST COMMERCIAL DESIGNATION |
|---|---|---|
| Resistors | | |
| R2016 | Ni Cr Metal Film, 1/8 Watt | XLT, IRC |
| R2048 | Tin Oxide Film, 1/8 Watt | NF60, Corning |
| Capacitors | | |
| R2045 | Fixed Glass Dielectric | CYFR, Corning |
| Diodes | | |
| R2008 P5, $P_{10}$ | Silicon, Regulator | IN751A, 758A, CDC |
| R2010 P1 | Silicon, VHF | IN251, CDC |
| R2011 P1 | Silicon, Computer | IN643A, CDC |
| R2013 P1 | Silicon, Low Current | IN647, PSI |
| Transistors | | |
| R2004 P1 | NPN, Silicon, 3 Watt | 2N1613 FSC |
| R2005 P1 | PNP, Silicon, 2 Watt | 2N1132 FSC |
| R2026 P1 | NPN, Silicon, 2 Watt | 2N708 FSC |
| R2050 P1 | NPN, Silicon, 4 Watt | 2N657 FSC |
| R4041 P1 | PNP, Silicon, 1 Watt | 2N869 FSC |

The parts under study were originally purchased for reliability evaluation during Project Advent (Contract AF04(647)-476). The reliability test and evaluation portion of the program was initiated to determine and specify procurement methods, screening techniques, and test and evaluation programs which would provide assurance that the hardware for the flyable satellites would meet the program objective of a 3-year life in a non-maintainable space environment.

The basic concepts upon which the long life parts program of Project Advent were initiated are as follows:

1. "There is a fully practicable design solution to the performance-life requirements of long life programs and this solution can be attained by thorough, meticulous attention to the proper design and application of selected and qualified materials, parts and components already known to the engineering fields."

2. "Stress-time relationships exist in nature which quantitatively define irreversible processes under normal use conditions and, when determined and evaluated, will provide assurance that the performance-life capability of the design is satisfactory for long life."

3. "Methods are available by which the variability of manufactured products can be adequately controlled in practice so that the quality and long life capability are not degraded below the level required for all parts, materials, components, and systems."

In consideration of these concepts and their application to long-life designs, an evaluation program to determine the life capability of electronic parts was formulated and testing initiated in 1961.

The necessity of providing assurance of minimum life-times of electronic parts for use in long life applications requires investigation in two major areas. The first involves the determination of the rate at which an electronic part will degrade or fail, and the second involves the development of tests for evaluating the homogeneity of parts (from the same lot) for conformity with an average rate of degradation or failure. Thus, the approach to providing assurance of long life reliability in electronic parts concerns itself with the development of degradation models and screening tests.

Thus, through investigations of cause and effect relationships, analyses of the physical and chemical make-up of the parts, and studies of the complex interactions of the various types of simultaneous loading it becomes possible to evaluate the inherent "load-carrying capability" of a part. Similarly, and more important in many ways, improvements in uniformity of product are possible through elimination of weak or non-homogeneous parts and correlations with the various control factors in the part manufacturing process.

The study of procurement methods for high reliability parts led to the establishment of the R-series high reliability parts specifications. The negotiations, quality assurance methods, and description of these specifications are shown in Section 4 of this report. The screening techniques established were presented and discussed in the Communications Satellite Project Advent Screening Tests Final Report (GE Document No. 63SD4250) and the Project Advent Final Technical Report.

Accelerated step stress and constant stress tests were performed on the parts during the Advent Program to provide data and information which would lead to the formulation of life test data, screening techniques, and accelerated test methods for long life programs. The test program continued until September, 1963 at which time the parts on life tests had accumulated 6,000 to 10,000 hours each at various conditions. The parts were then placed at storage conditions of 25°C and zero power for nine months and were reactivated to prior test conditions in June, 1964 as a requirement of this program. The step stress tests which were completed during the Advent Program provided data which were to be analyzed for this project. The combination of the step stress tests and the constant stress tests are to form the basis for the determination of the measurement techniques for controllable accelerated testing under this present program.

The definition and establishment of accelerated testing methods and techniques for electronic parts must be based upon the actual failure mechanisms which exist in the part. Consequently this program consists of two distinct yet interrelated investigations. The presentation of the accelerated testing concept, approach and results to date are shown in Section 2. The results of the studies of the failure mechanisms to date are shown in Section 3.

The Summary and Conclusions are presented in Section 5 and the Program for the Next Reporting Period is shown in Section 6.

BLANK PAGE

# 2. ACCELERATED TESTING TECHNIQUES

## 2.1 INTRODUCTION

A review of the existing data and test design of the Project Advent parts testing program was made for the purpose of using the information and adopting the techniques for use on the RADC program. All available parts test data have been key punched for automatic data processing and run-offs of the data are in the process of being incorporated into the reliability control files at RADC.

Table 2-1 presents a summary of the Advent Test Program showing the part type, the test conditions, and the quantity on test.

## 2.2 DESCRIPTION OF TEST PROGRAM

### 2.2.1 General

Figure 2-1 illustrates the general test pattern used on the Advent Test Program. Modifications were made in the step stress phases as described in Paragraph 2.7. The stress levels, times at stress, and the part parameters selected for each part type are unique to each part type and are based upon the expected degradation mechanisms.

Table 2-2 presents a summary of the Test Specifications used for this program. Each test specification contains the test objective, description of the part, mounting requirements, preliminary screening tests, failure criteria, and description of each phase of the test. A general test specification GTS-AD1, was also issued describing the common requirements applicable to the testing program. Each test specification is designed to provide a thorough demonstration of the part degradation mechanisms and the patterns of behavior of the part on test.

Externally produced, uniformly and accurately applied thermal energy was selected as the degradation inducing stress for resistors and semiconductors. This selection was based upon the fact that changes in the electrical properties of these types of electronic parts, with respect to time, are the result of chemical and physical changes, which are usually accelerable by the application of thermal energy to the part. The simultaneous application of 50 percent of the manufacturer's rated power (calculated for a case temperature of 50°C) to these parts was made to accentuate film imperfections and accelerate diffusion of ionizable impurties.

TABLE 2-1. PART EVALUATION PROGRAM

| | Phase: I | II | III | IV | V | VI | 25 C | Total |
|---|---|---|---|---|---|---|---|---|
| **Resistors** | | | | | | | | |
| R2016P1002 | 25 | 20 | - | 19 | 18 | - | - | 82 |
| P1003 | 25 | 50 | 50 | 50 | 50 | - | 150 | 375 |
| P2002 | 25 | 50 | 50 | 50 | 50 | - | - | 225 |
| R2048P1002 | 25 | 100 | 50 | 50 | 50 | - | 500 | 775 |
| P1003 | 25 | 100 | 50 | 50 | 50 | - | 250 | 525 |
| R2016P1001 | - | - | - | - | - | 25 | - | 25 |
| R2048P1001 | - | - | - | - | - | 50 | - | 50 |
| R2049P1001 | - | - | - | - | - | 25 | - | 25 |
| XLT 100 K ohm | - | 100 | - | - | - | - | - | 100 |
| R2048P1001 | Uncased - $10^{-6}$ mm Hg Failure Mechanism Study Tests | | | | | | | 10 |
| | | | | | Total Resistors | | | 2192 |
| **Capacitors** | | | | | | | | |
| R2045P102 | - | - | - | 20 | 20 | 20 | - | 60 |
| R2045P122A | - | - | - | 20 | 20 | 20 | - | 60 |
| R2045P151 | 25 | 25 | 25 | 25 | 25 | 25 | 20 | 170 |
| P101 | - | - | - | - | - | - | 20 | 20 |
| P271 | - | - | - | - | - | - | 20 | 20 |
| P680 | - | - | - | - | - | - | 40 | 40 |
| R2024P1R0 | - | - | - | - | - | 25 | - | 25 |
| R2023 Prototype | Vacuum life test - $10^{-6}$ mm Hg-Abs. | | | | | | | 40* |
| R2045P151 | Failure Mechanism Study Tests | | | | | | | 96 |
| | | | | | Total Capacitors | | | 531 |
| **Diodes** | | | | | | | | |
| R2008P5 | 50 | 50 | - | 48 | 48 | - | 60 | 256 |
| P10 | - | - | - | 50 | - | - | 99 | 149 |
| R2010P1 | 50 | - | - | 50 | 50 | 50 | 75 | 275 |
| R2011P1 | 100 | - | - | 50 | 50 | 50 | 400 | 650 |
| 019M | (60) prototype of R2012 | | | | | | | 60 |
| R2013P1 | 60 | - | - | 25 | 21 | - | - | 106 |
| R2010P1 | Failure Mechanism Study Tests | | | | | | | 19 |
| | | | | | Total Diodes | | | 1515 |
| **Transistors** | | | | | | | | |
| R2004P1 | 25 | - | - | 99 | 50 | - | 50 | 224 |
| R2005P1 | 50 | - | - | - | - | 50 | 25 | 125 |
| R2026P1 | 25 | - | - | 49 | 50 | 50 | 50 | 224 |
| R2050P1 | 50 | 50 | - | 50 | 50 | - | 50 | 250 |
| 2N335 | Life vs thermal resistance | | | | | | | 50* |
| 2N1450 | Life vs thermal resistance | | | | | | | 50 |
| 251M | Prototype for R2047; reverse bias test | | | | | | | 25 |
| R4041 | - | - | - | 50 | 50 | | | 100 |
| | | | | | Total Transistors | | | 1048 |
| | | | | | TOTAL ALL PARTS ON TEST (6/1/63) | | | 5286 |

Incoming inspection and screening tests were performed on all R-xxxx parts listed above.

*Tests started before 6/1/62.

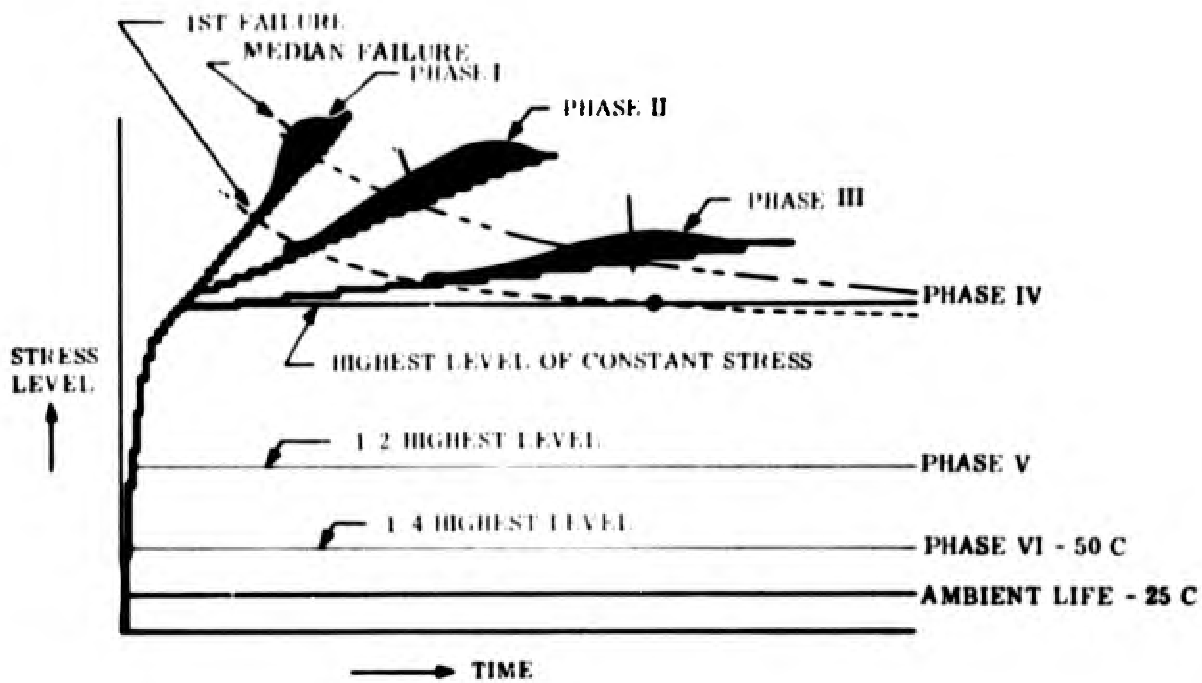


Figure 2-1. General Test Plan

TABLE 2-2. TEST SPECIFICATIONS

| PART NO. | TYPE | SPECIFICATION NO. |
|---|---|---|
| R2016 | Metal Film Resistor - 1/8 Watt | S-32016 |
| R2048 | Oxide Film Resistor - 1/8 Watt | S-32048 |
| R2008 | Regulator Diode, Silicon | S-32008 |
| R2010 | VHF Diode, Silicon | S-32010 |
| R2011 | Computer Diode, Silicon | S-32011 |
| R2013 | Low Current Diode, Silicon | S-32013 |
| R2004 | 3 Watt, NPN Silicon | S-32004 |
| R2005 | 2 Watt, PNP, Silicon | S-32005 |
| R2026 | 2 Watt, NPN, Silicon | S-32026 |
| R2050 | 4 Watt, NPN, Silicon | S-32050 |
| R4041 | 1 Watt, PNP, Silicon | S-34041 |

Since thermal energy was selected as one of the degradation inducing stresses for the majority of the tests, the necessity for precisely controlling and measuring the critical element temperature of the part is of prime importance. The control is accomplished by:

a. Design and use of special mounting fixtures for the parts on test,

b. Measurement of the thermal resistance of semiconductors placed on test,

c. Use of ovens with a ±2°C temperature control for high temperatures and use of oil baths with a ±1/2°C control for lower temperature life tests, and

d. Use of a nitrogen atmosphere in the ovens to retard oxidation of leads.

The evaluation tests on the parts are being performed in accordance with the specifications listed above at the General Electric Spacecraft Department Part Test Laboratory. The tests are run continuously (24-hour day, 7-day week) where required.

Prior to starting each test, detailed test instructions were written by the Parts Laboratory Test Engineer for use by the test technicians. In preparing these instructions, all questions of test plan interpretation were reviewed with cognizant personnel so that the intent of the test plan would be fulfilled.

When the test is ready to start, the complete test procedure and set-up is reviewed by the Parts Laboratory technicians and engineering personnel. After every parameter measurement the data are reviewed by engineers responsible for the test prior to starting on the next measurement interval.

All parameter measurements data are key punched for Automatic Data Processing. Computer programs are established for manipulation of the data and copies of the reduced data are distributed to those concerned with the analysis of the test results.

Parts which fail during the test and those parts which complete the test are taken to the tear-down laboratory where various analysis techniques are used to identify the degradation mechanisms exhibited during the tests. Comparison studies and tests are performed on similar parts in the Failure Analysis Laboratory where the expected part degradation mechanisms are determined.

All the above information is accumulated by engineering personnel, then detailed parameter trend analysis is performed and the results are presented in a manner suitable for use by engineers associated with the life capability of electronic parts.

### 2.2.2 Details of Test Program

The parts on constant stress test Phases IV, V, VI and ambient life have been measured and the test restarted. The Advent tests continued for several hundred hours after the last parameter readings were taken. Some changes from the previous readings were observed in the parts on Phase IV tests, presumably because of this additional test time. No significant changes were observed in parts on the other tests after approximately nine-months storage.

New test plans were issued for Phases I, II and III. Changes from the Advent plans are: use of the same temperature steps on all three phases, temperature steps arranged to be equal on a 1/T absolute basis, current noise measurements on all semiconductors, capacitance measurements on semiconductors, measurements of $I_R$ to -65°C on four R2008P10 diodes at each stress step, and changes in the length of the steps necessitated by work scheduling in the Parts Test Laboratory.

The semiconductors have been divided into two groups of 25 each. One group has the voltage (but not the current) maintained during the oven cooling period at the end of each step stress period. The other group is completely turned off during cooling. The purpose of this is to determine whether the device surfaces recover significantly during the time they are at high temperature with no voltage applied.

Several changes have been made in the operation of the tests. Nitrogen is used as the atmosphere in the high temperature oven to minimize oxidation of the leads and connectors which affected parameter measurements in the previous tests. An upper limit of 350°C for resistors and 300°C for semiconductors was set because changes in failure mechanism were observed to occur at higher temperatures.

The mounting of the semiconductors has been changed to give more uniform heat conditions throughout the step stress tests. Under-voltage relays have been placed in the 115 volt lines to all power supplies. If the power fails, the relays drop out and must be reset manually. This will eliminate the possibility of voltage surges due to automatic start-up which are particularly harmful to semiconductors.

Table 2-3 lists the parts that have been screened and started on the step stress tests.

In order to increase the confidence level at a given set of stress conditions the sample size for the step stress tests was doubled, that is from 25 to 50. An additional 10 rejected or unscreened parts were also placed on test. These should provide an indication of the value of the screening tests.

TABLE 2-3. STEP STRESS TESTS

| PART | PHASE | NUMBER ON TEST | STATUS |
|---|---|---|---|
| R2016P1003 | I | 50 (10 unscreened) | Completed |
| R2016P1003 | II, III | 50 (10 unscreened) | III Under Way<br>II Sched - 10/16 |
| R2008P10 | I | 50 (10 unscreened) | Completed |
| | II, III | 50 (10 unscreened) | Under Way |
| R2010P1 | II, III | 50 (10 unscreened) | Under Way |
| R2011P1 | II, III | 50 (10 unscreened) | Under Way |
| R2026P1 | II, III | 50 (10 unscreened) | Under Way |
| R2050P1 | II, III | 50 (10 unscreened) | Under Way |

## 2.3 GENERAL ANALYSIS APPROACH

In general, it may be stated that the lifetime of a device is the time during which no measurable parameters exceed established limit values. The cessation of "life" may occur in either of two ways. First, it may occur at a measurable rate of degradation when a measurable part parameter exceeds established limits, as in the case of resistance drift of a resistor; second, it may occur catastrophically without prior measurable parameter variations when the applied stress (environment stress plus operating stress) exceeds the strength of the device, such as in dielectrics which fail due to sudden dielectric breakdown.

Graphically, each of these conditions may be illustrated as follows:

1. Deterioration of Part Parameter

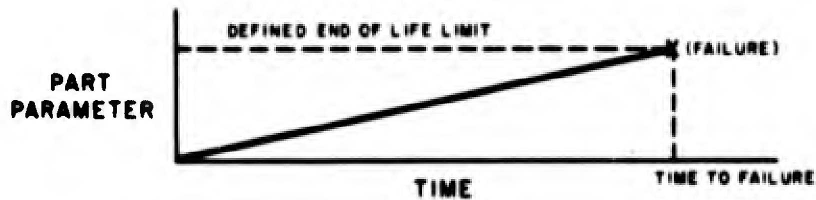


2. Degradation of Ultimate Strength

The drift of a part parameter beyond an arbitrary end-of-life limit does not necessarily mean that a system would be completely inoperative. The failure mentioned here means only that the system must compensate for the parameter drift in some way and in a non-maintainable space vehicle alternative fixes are very few. However, this type of failure may not have as serious consequences on the success of a vehicle as a catastrophic failure, that is a short or open circuit.

2.3.1 Deterioration of Part Parameter

For deterioration type failures, the rate of reaction of the degradation mechanism which governs the changes of the part parameter must be determined in order to provide an estimate of the time during which the parameter remains within the established limit.

The approach taken for this program is to assume that the drift of the part parameter is chemical in nature, thus the relationship of reaction rates and temperature expressed by the Arrhenius Equation may be used:

$$R = a e^{-\frac{b}{KT}} \tag{1}$$

This relation was developed empirically and was criticized on the basis of being dimensionally incorrect. H. Eyring developed from theoretical considerations a dimensionally correct equation which included a stress term in addition to temperature. The reaction rate (R) expressed by the Eyring relation is written as follows:

$$R = R_o e^{nS} = a_1 T^w e^{-\frac{b}{KT}} S \left(c + \frac{d}{KT}\right) \tag{2}$$

Where

$R_o$ = degradation rate in the absence of applied stress

K = Boltzman's constant

T = Absolute temperature of the active element

a, $a_1$, b, c, d, and w = Undetermined part constants independent of time, temperature, and stress

S = A function of the applied stress

$n = c + \frac{d}{KT}$

The total change which a part incurs during a period of time is equal to the product of the rate of degradation and time under consideration.

Thus:

$$D_T = Rt + c \tag{3}$$

t = time

c = initial damage or "zero" value

$D_T$ = Total Damage (some function of a measurable past parameter)

In the analysis of data generated in this program a function of damage which is linear with time (t) is sought. This will enable the design engineer to estimate the damage that will occur during any time under a given set of application stresses and environments.

When testing parts and materials which have a long-life capability, it is necessary to use accelerated test methods to provide the damage-time relationship. For the step stress method of accelerated testing the damage function for each of several rates of stress increase is plotted versus a function of stress to yield a linear relationship for each test. Changes in the slope of the line will indicate changes in the rate of damage accumulation and thus in the failure mechanism. Similar plots are made for high level constant stress accelerated tests. From the damage versus stress curves the times to reach particular levels of damage can be determined. These values may then be plotted as design life data charts (damage vs time). Extrapolation of the straight lines to application stress levels (longer times, are valid when the rate of reaction of the degradation mechanism remains constant, Equation 3.

### 2.3.2 Degradation of Ultimate Strength

The ultimate strength of any single device is impossible to measure directly without destroying it. In this case, a statistical approach, based on lot sampling or the use of damage sensitive secondary measurements, is necessary for estimation of average lifetimes.

The average rate at which the ultimate strengths of the parts degrade must be determined by a series of accelerated tests-to-failure. These test results may then be used to establish the life characteristics of the part type with statistical confidence limits.

Accelerated tests, using both the step stress and constant stress techniques, are used in this program for this type of failure also. For the step stress method, the stress function (for each of several rates of stress increase) is plotted versus a cumulative probability scale. It is generally possible to find a stress function and a probability scale which will result in a straight line plot.

Percentile points taken from the probability plot are then plotted as stress versus the time of the stress step to provide design data charts. When extrapolated to the application stress level the percent failure to be expected at any time interval can be found, provided the failure mechanism remains the same.

The assumptions made for each of the above conditions will be modified by such phenomenon as diffusion rates and electrical field effects. These additional factors must be considered in the test design and analysis for each part type and its projected use. The generalizations given above provide the basis for the approach to test design and analysis which are shown in more detail in the following paragraphs.

## 2.4 ANALYSIS PLAN

The analysis of the data from the step stress and constant stress tests of the parts, is based upon testing hypotheses generated in consideration of the chemical degradation

theory presented above. Basically, there are two general approaches to the plotting and presentation of the data which were developed using the general test plan of Paragraph 2.2. Each method has its unique technique which are shown in detail below.

### 2.4.1 Parts Where Deterioration can be Measured

Determine a damage parameter which will be linear (may require a transformation) when plotted against 1/T in degrees K.

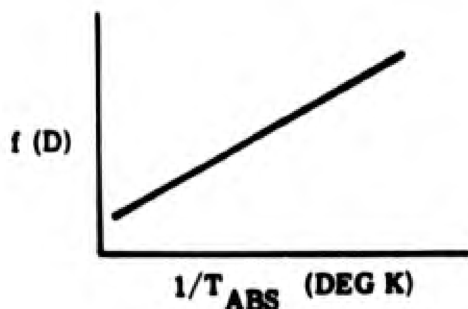


The determination of the damage relationship for film resistors which gives a linear relationship when plotted against 1/T is shown in Paragraph 2.7.1.

Perform a series of step stress tests-to-failure and plot the results in the following manner:

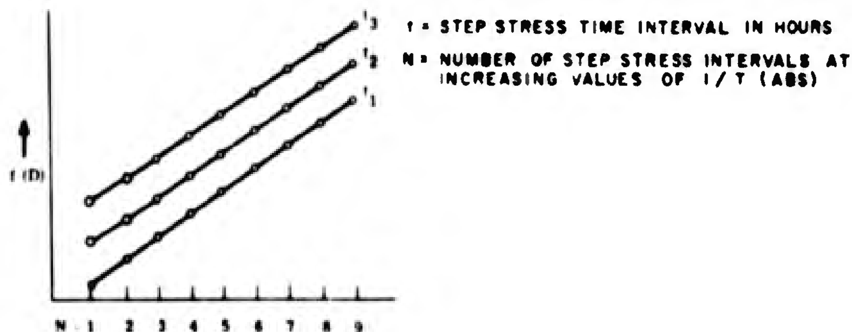


The slopes of the lines should be identical when the chemical mechanism producing the deterioration of the damage parameter for each step-stress is the same.

2.4.1.1 From the above plot, determine the damage values for constant temperature and step stress time. Plot the readings for constant damage lines in a 1/T vs time chart.

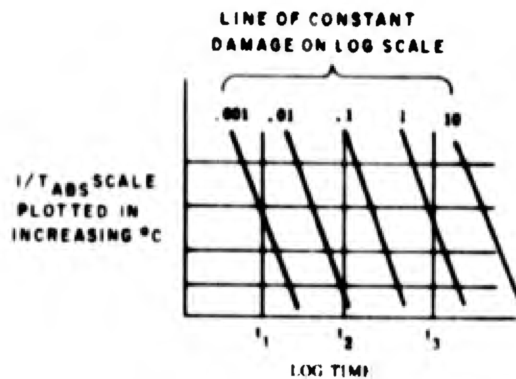


2.4.1.2 Changes in failure mechanism will appear as follows:

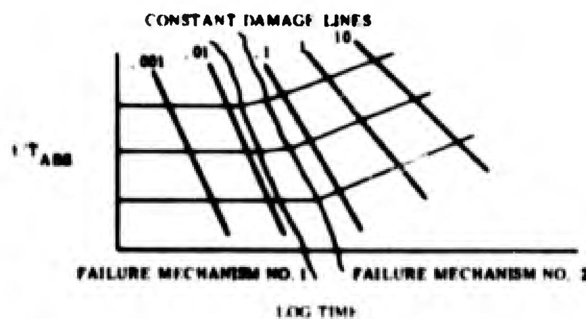


2.4.1.3 Long term constant stress test results may be plotted on the same type format. Changing failure mechanisms in constant stress tests will yield a plot similar to 2.4.1.2. Correlation mathematics for relating the step-stress and constant stress tests must then be developed.

2.4.1.4 Develop charts which show the damage accumulation rate for stress tests during screening (burn-in tests).

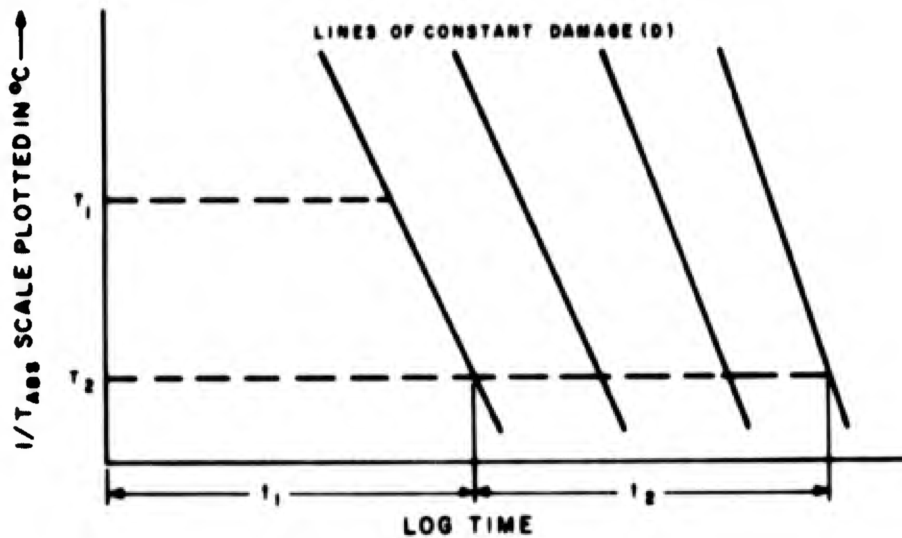


$T_1$ - Burn-in temperature

$T_2$ - Maximum use temperature

$t_1$ - Portion of part life time used up by screening test

$t_2$ - Remaining part life time to a given failure definition of specified damage.

2.4.2 Parts Whose Failure are Catastrophic

2.4.2.1 Perform a series of step stress tests-to-failure and plot the results in the following manner:

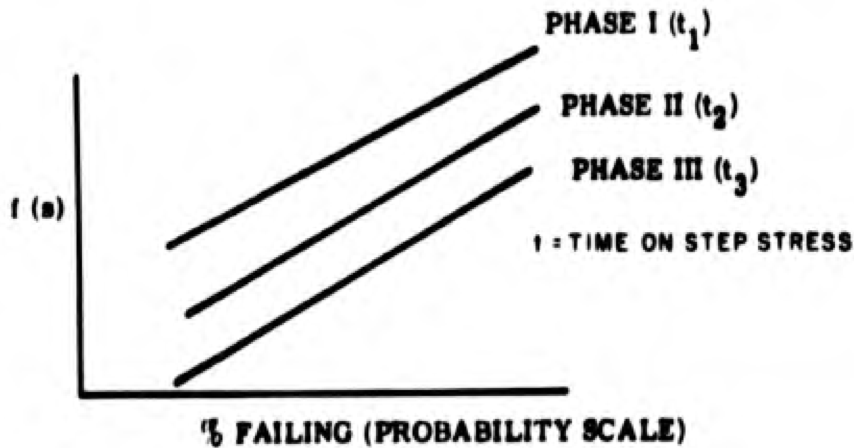


Various probability scales may be tried until some function of applied stress and percent failure yield a linear fit. The line may have changes in slope which indicate changes

in failure mechanisms. The three phase tests should also be of the same slope showing only the effect of the increased time of the different test phases.

The Probability Scale used for capacitor tests is Weibull and for semiconductor tests is either normal or log-normal.

2.4.2.2 Plot applied stress versus step stress time.

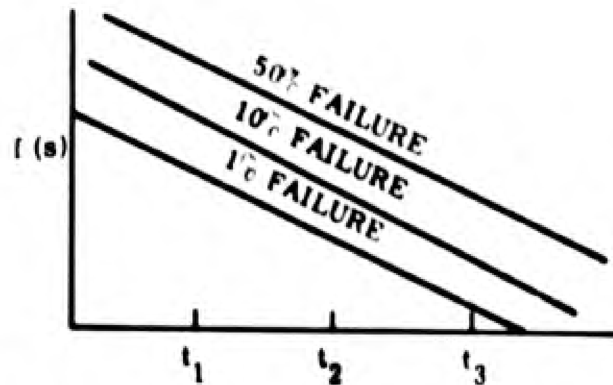


2.4.2.3 Long term constant stress test results may be plotted in the same format and tested for correlation with step stress results.

2.4.2.4 Develop Design Life Data Charts.

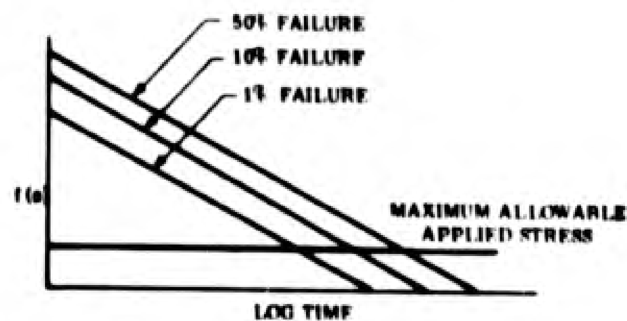


f(s) for capacitors is applied voltage on a logarithmic scale

f(s) for semiconductors is a $1/T_{ABS}$ scale with a reverse bias applied to junction.

2.4.2.5 Develop Screening criteria.

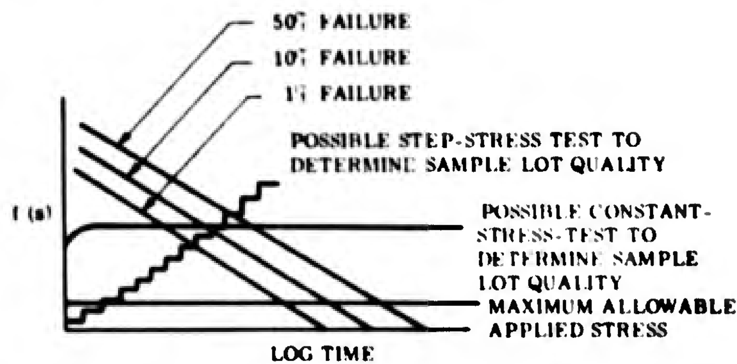


Proof tests may be made on sample from lot.

## 2.5 RELATIONSHIP OF PROGRESSIVE STRESS AND CONSTANT STRESS

The results of tests on capacitors using progressive stress techniques have been correlated with those using constant stress techniques*. This correlation is based upon the following assumptions:

1. The decrease in strength of parts under stress is due to the "damage" done to the parts by the stress over the period of time the parts are subjected to the stress.

2. The failure of homogeneous parts occurs after a fixed amount of damage has accumulated regardless (within practical limits) of the rate at which that damage occurs.

Upon this basis, data from accelerated life tests of mica capacitors, taken in sample sizes of 250 specimens along each of a considerable number of different constant stress levels or rates of rise, have been correlated.

Let s denote the stress level, $d_0$ the initial damage, and f(s) dt denote the damage done during testing to the (homogeneous) part in time dt. At time t the accumulated damage D(t) may be expressed as

$$D(t) = \int_{t_0}^{t} f(s)\, dt + d_0 \qquad (4)$$

*H.S. Endicott, J.A. Zoellner, A Preliminary Investigation of the Steady and Progressive Testing of Mica Capacitors, Seventh National Symposium on Reliability and Quality Control, Philadelphia, Pa., Jan 9-11, 1961, pgs 229-240.

Failure of an individual part will result when $D(t) \geq D_c$, a critical value for damage. Both $D_c$ and $d_o$ vary from unit to unit and depend upon manufacturing variations and material and design limitations.

Test results from many tests of both materials and parts* have shown that "life" is inversely proportional to some power (n) of the applied constant stress. That is

$$\frac{t_1}{t_2} = \left(\frac{S_2}{S_1}\right)^n \tag{5}$$

When this is the case, $f(s) = S^n$ damage accumulates linearly with time. The total damage accumulated during test to failure is

$$D(t_f) = \int_{t_o}^{t_f} S^n \, dt = S^n \left(t_f - t_o\right) \tag{6}$$

If, instead of applying a constant level of stress, the stress level is uniformly and continuously increased from zero, S is a function of time. Where r is the rate of increase of stress level S as a function of time t, then $S^n = r^n t^n$ and the damage is

$$D(t_f) = \int_{t_o}^{t_f} r^n t^n \, dt = \frac{r^n}{n+1} t_f^{\,n+1} - \frac{r^n}{n+1} t_o^{\,n+1}$$

If $t_o = 0$, then

$$D(t_f) = \frac{1}{n+1} S_f^{\,n} \, t \tag{7}$$

Thus, where the parts are homogeneous and the damage at failure is the same regardless of the rate at which the damage occurred, the two expressions for damage, Equations 6 and 7, may be equated, and

$$S_{c_f}^{\,n} t_f \text{ (at constant stress)} = \frac{1}{n+1} S_{p_f}^{\,n} t_f \text{ (at progressive stress)} \tag{8}$$

---

*H.S. Endicott, J.A. Zoellner, A Preliminary Investigation of the Steady and Progressive Testing of Mica Capacitors, Seventh National Symposium on Reliability and Quality Control, Philadelphia, Pa., Jan 9-11, 1961, pgs 229-240.

When the value of n has been determined, the results from an increasing (or progressive) stress test may be used to calculate the equivalent constant stress values or time to failure.

## 2.6 RELATIONSHIP OF STEP STRESS AND CONSTANT STRESS

The relationship of step stress and constant stress has been derived* in a manner similar to that shown above for progressive stress and is expressed by the following equation:

$$t_c = K \frac{V_m^{\,n}}{V_c} \, t_{ss} \, \frac{m}{n+1} \qquad (9)$$

Where

$m$ = number of steps

$t_{ss}$ = time of one step

$K$ = a correction factor which var'es with m

| m | K |
|---|---|
| 1 | 15.7 |
| 2 | 5.53 |
| 3 | 3.73 |
| 4 | 2.90 |
| 5 | 2.45 |
| 7 | 1.97 |
| 10 | 1.64 |
| 20 | 1.30 |
| 23 | 1.26 |
| 24 | 1.24 |

As the number of steps is increased to infinity, Equation (9) reduces to Equation (8); that is, $m\, t_{ss} = S_p$ and $K = 1$.

---

*H.S. Endicott, B.D. Hatch, R.G. Sohmer, Application of the Eyring Model to Capacitor Aging Data, to be published in IEEE Transactions, date 1964 or early 1965.

## 2.7 ANALYSIS OF ADVENT TEST DATA

### 2.7.1 Resistors

The purpose of the resistor test program stated in Test Specifications S-32016 and S-32048 is to induce the failure mechanisms of each of two types of film resistors at several rates. Each specification requires that a series of six tests be performed — three step stress tests at different rates of stress and time interval increase and three constant stress tests at different levels of stress. The parts which were placed on test have been fully controlled to General Electric High Reliability Specifications R-2016 and R-2048. The screening tests specified were performed in the Parts Testing Laboratory.

2.7.1.1 Approach to Testing — Briefly, the step stress approach consists of considering stress as the independent variable and some function of damage as the dependent variable of deterioration. Instead of measuring the time to failure, the procedure is to measure the temperature at which deterioration, observed in terms of change in resistance (damage), becomes significant. Starting at a stress level where deterioration is known not to be significant the stress is increased in increments and maintained for a specified period of time.

Phases I, II and III of the test program consisted of incremental steps of stress and time durations designed to induce failure rapidly; Phase I at the fastest rate, Phase II at 1/10 of Phase I, and Phase III at 1/10 of Phase II. Phase II repeats Phase I conditions to a level about 80 percent of that at which the first Phase I failure occurred prior to proceeding at Phase II rate of stress application. Phase III repeats Phase I conditions in a similar manner. This is done so as to accumulate as much of the same "preconditioning" effects as possible. The purpose of the elevated and rated constant stress test (Phases IV, V and VI) is to generate data which will enable the hypothesis of "long life predictability from short term tests" to be investigated.

Thermal energy, precisely controlled and measured, was selected as the stress because deterioration of the resistor's active element (i.e., the resistive film) is realistically accelerable by heat. The necessity of uniformly applying the heat resulted in the design of special mounting fixtures and the application of externally generated heat. The resistors were tested with an applied voltage which was 50 percent of the manufacturer's power rating. This was done so as to accentuate the effect of any structural defects or imperfections of the resistor. In addition a test environment was created which was not entirely unrelated to usage conditions and which included the electrical contribution to the deterioration of the resistors active element.

Degradation of a resistive device primarily stems from permanent changes in its internal state. The change in the internal state is reflected by changes in a structure sensitive property such as resistance.

Resistance ($R_1$) measured at a temperature T, is defined by:

$$R_1 = R_o \ (1 + \alpha \Delta T + \beta \Delta T^2 + \ldots), \quad (10)$$

where

$R_o$ = resistance measured at reference temperature, usually 25 C

$\Delta T$ = temperature difference between the temperature at $R_f$ and $R_i$

$\alpha$, $\beta$, etc. = temperature coefficients.

Damage or degradation of a resistor is assumed to be primarily reflected in changes in $R_o$. This term ($R_o$) may be expressed as the product of the specific resistivity and a geometry correction factor. Changes in $R_o$ may be expected since changes in the crystalline structure of the resistor material due to heat treatment, mechanical strain, or impurities alloyed with the material, even in minute quantities, may have a pronounced effect on its resistivity and in turn on its $R_o$ value.

Consider the case of a constant elevated temperature stress condition:

where,

$R_i$ = Resistance at beginning of stress

$R_f$ = Resistance at end of stress

$R_{oi}$ = Resistance at reference temperature at beginning of stress

$R_{of}$ = Resistance at reference temperature at end of stress

Then

$$R_f = R_{of} \ (1 + \alpha \Delta T + \beta \Delta T^2 + \ldots) \quad (11)$$

$$R_i = R_{oi} \ (1 + \alpha \Delta T + \beta \Delta T^2 + \ldots)$$

The damage (D) or permanent set in the resistance value at reference temperature is:

$$D = \frac{R_f - R_i}{R_i} = \frac{R_{of} - R_{oi}}{R_{oi}} \quad (12)$$

Thus, through the use of above ratio, an appropriate measure of damage can be determined independent of temperature effects.

Since damage reflects permanent changes in the internal state of a device, by virtue of it's nature, it is irreversible, i.e., unidirectional under normal use conditions, and is measured by the total activity of a device. In order to indicate the total physicochemical reaction that is taking place, the total damage that occurs in a resistor is indicated by the total change in resistance. The ratio is expressed as an absolute value to account for any opposing sense of $\beta$ which may become dominant at higher temperatures and the change in reaction rates in time.

Therefore;

$$D = \frac{|R_{of} - R_{oi}|}{R_{oi}} \tag{13}$$

In step-stress testing where thermal energy is the applied stress,

$$D_T = \sum_{j=1}^{N} \left\{ \frac{|R_{of} - R_{oi}|}{R_{oi}} \right\}_j \tag{14}$$

where, j refers to the step-stress number (j = 1, 2, 3 ... N).

2.7.1.2 Analysis of Data — The data developed during the Advent parts evaluation program have been processed by computer, including the data accumulated following the Advent final report. The data printouts show the matrix of input resistance values for each time interval; matrix of sums of delta resistance values; matrix of sums of absolute delta resistance values; and the maximum, minimum, average and standard deviation of each of the above for each reading interval.

The step stress data have been processed similarly except that temperature intervals rather than time intervals have been used for the parameter reading periods.

For analysis of the resistor data both W and S in the Eyring equation (Equation 2) are considered to be zero. The equation thus reduces to:

$$R = a_1 e^{-\frac{b}{kt}} \tag{15}$$

where $a_1$ = frequency factor of molecular encounter.

This form of the Eyring model will be recognized as the form of the Arrhenius equation.

The concentration of a reacting substance is related to the chemical reaction rate as follows:

$$-\frac{dc}{dt} = kc^n \tag{16}$$

where n is the order of the chemical reaction.

For a zero order chemical reaction n = 0, and integration of Equation 16 gives the following:

$$c = k\,t + \text{constant} \tag{17}$$

For a first-order chemical reaction n = 1, integration and converting to logarithms gives

$$\ln c = -kt + \text{constant} \tag{18}$$

The order of the reaction involved in changes in resistance values is not known. Some mechanical processes have been found to have a zero-order reaction rate wheras organic insulation deterioration has been found to have a first-order reaction rate.

In order to apply either of these equations, it is necessary to assume that some property of the resistors is a function of time and is proportional to a constituent that is a measure of deterioration in a manner analogous to the concentration of a reacting substance and the reaction rate, that is c = f (Resistance). The appropriate function of resistance must still be determined.

The dependence on temperature is shown by substituting the value of k from Equation 15 into Equations 17 and 18, respectively

$$c = -Ate^{-\frac{E}{RT}} + C \tag{19}$$

$$\ln c = -Ate^{-\frac{E}{RT}} + C \tag{20}$$

Taking logarithms and transposing

$$\ln t = \ln\left(\frac{C-c}{A}\right) + \frac{E}{RT} \tag{21}$$

$$\ln t = \ln\left[\frac{C - \ln c}{A}\right] + \frac{E}{RT} \tag{22}$$

where C is the value of c or of ln c, respectively, when t = 0.

Equations 21 and 22 are in the form

$$\ln t = a + \frac{b}{T} \tag{23}$$

Figure 2-2 illustrates the relation of "damage" to the reciprocal of absolute temperature for the R2016P1003 resistor, Phases I, II and III. Horizontal lines in the plot are equal damage lines. The temperatures for equal damage have been replotted in Figure 2-3 to show the relation of time and reciprocal of absolute temperature.

The 0.5 percent damage line has been used to determine the constants a and b in Equation 24.

$$\log t = \frac{4306}{T} - 6.544 \tag{24}$$

The time required at a constant temperature to give the same damage as a step stress test can be easily calculated when the slope is known.

$$t_{\text{constant temp.}} = t_{\text{per step}} \frac{\sum_{T_i}^{T_n} e^{-\frac{E}{RT_i}}}{e^{-\frac{E}{RT_{(\text{constant temp})}}}} \tag{25}$$

where, $T_i$ = 1st temperature step.

Regardless of the form of f (resistance), the term in Equations 21 and 22 corresponding to a in Equation 23 will be a constant for a particular end point of resistance change.

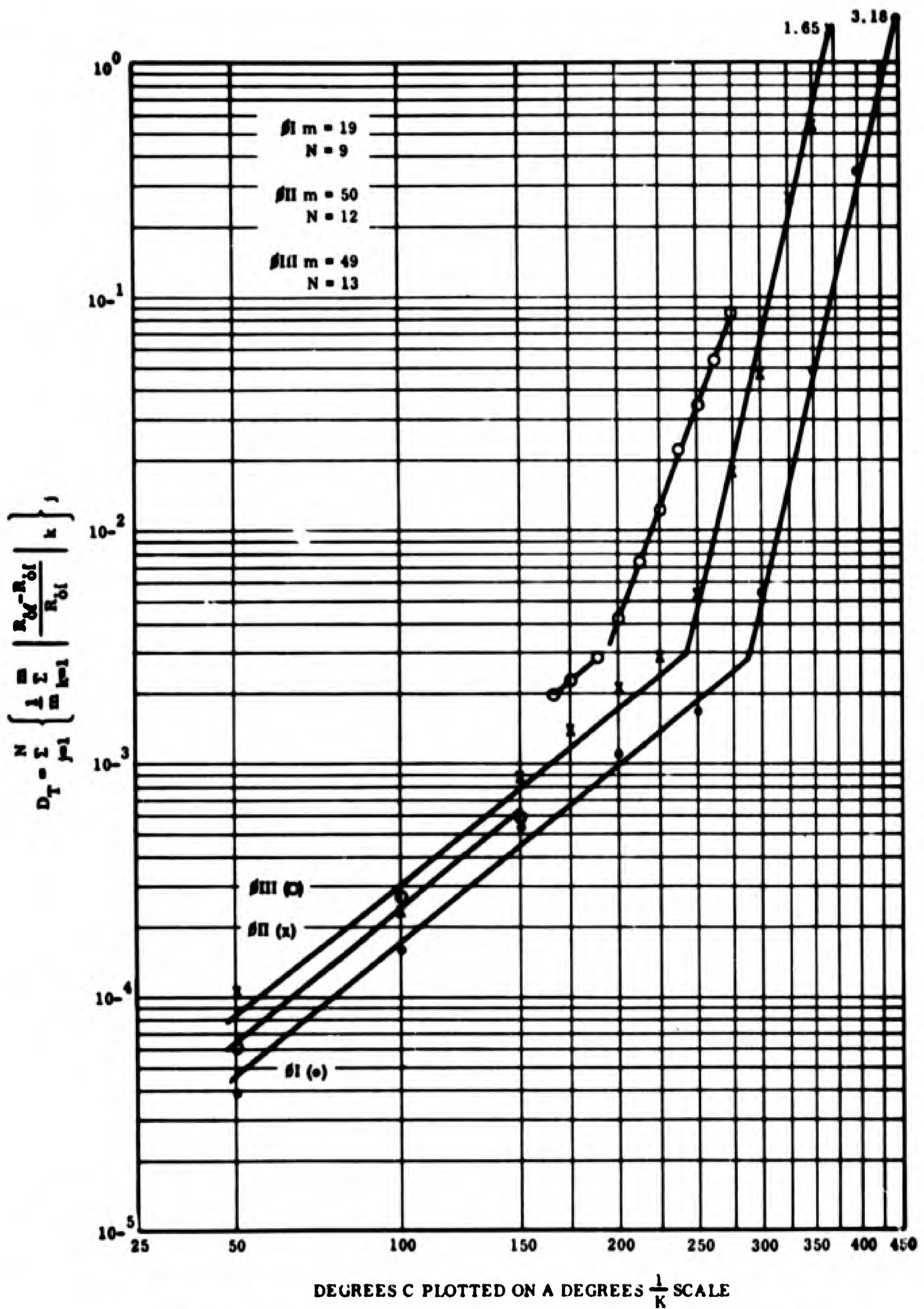


Figure 2-2. R2016P1003 - Phase I, II and III Damage Relationships

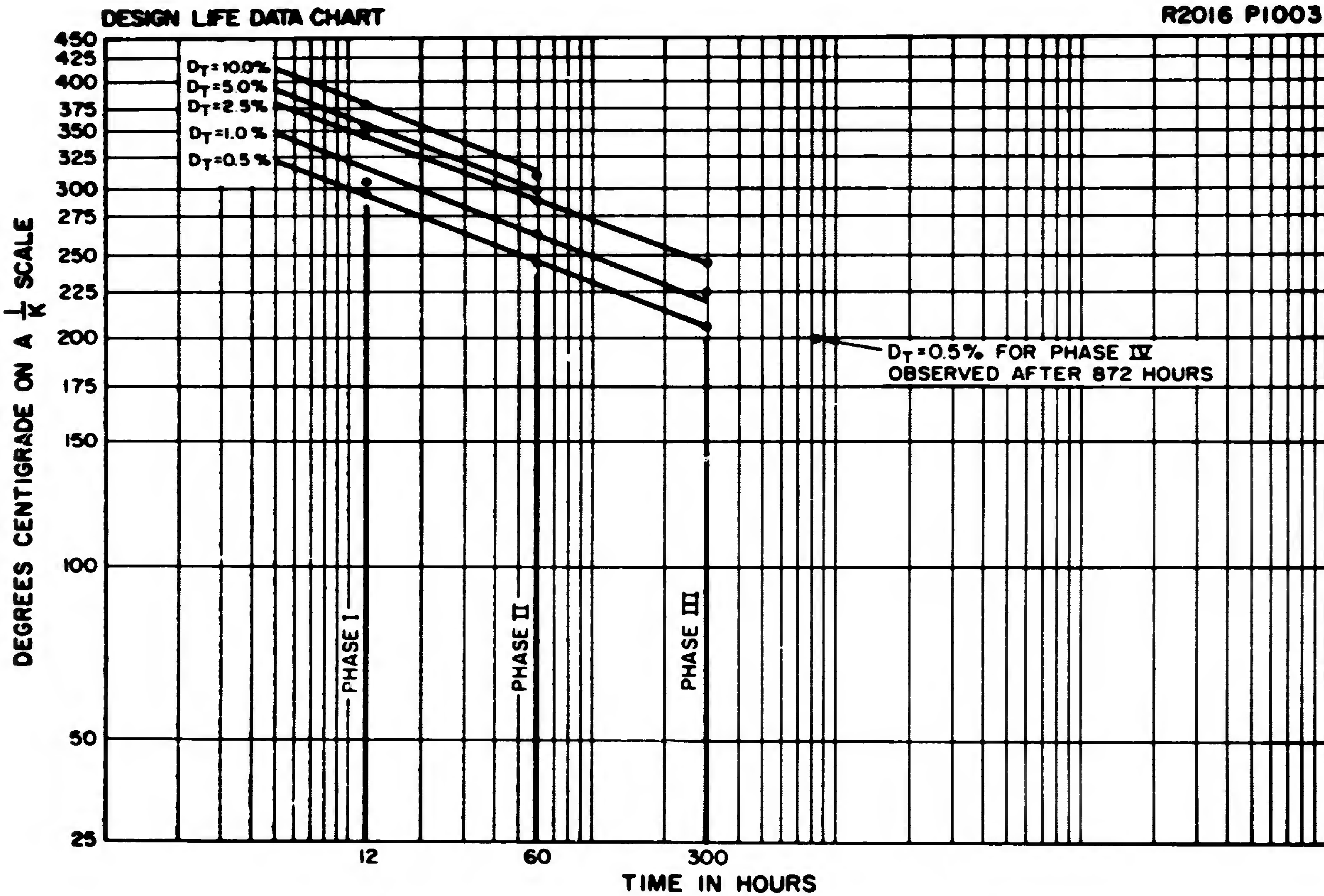


Figure 2-3. R2016P1003 - Design Life Data Chart

An example of the constant stress data which has been generated is given in Table 2-4 for the Phase IV test of the R2016P1003 resistors. Phase IV is being performed at an ambient temperature of 200°C with 79 volt dc applied to the resistor. The maximum, minimum and average values of resistance are plotted in Figure 2-4.

TABLE 2-4. R2016P1003 PHASE IV (200°C - 70 VOLTS DC)

| HOURS | AVERAGE | MAXIMUM | MINIMUM |
|---|---|---|---|
| 0 | 100.062 | 100.710 | 98.890 |
| 24 | 99.992 | 100.700 | 98.790 |
| 168 | 99.873 | 100.590 | 98.690 |
| 504 | 99.588 | 100.220 | 98.549 |
| 1008 | 99.531 | 100.170 | 98.479 |
| 1508 | 99.584 | 100.250 | 98.513 |
| 2011 | 99.455 | 99.999 | 98.399 |
| 2508 | 99.526 | 100.000 | 98.469 |
| 3008 | 99.579 | 100.150 | 98.563 |
| 3501 | 99.577 | 100.190 | 98.522 |
| 4008 | 99.692 | 100.190 | 98.559 |
| 4515 | 99.658 | 100.190 | 98.600 |
| 5012 | 99.602 | 100.150 | 98.557 |
| 5512 | 99.657 | 100.200 | 98.592 |
| 6012 | 99.650 | 100.210 | 98.582 |
| 6512 | 99.673 | 100.170 | 98.610 |
| 7022 | 99.599 | 100.010 | 98.569 |
| 7550 | Test shut down<br>Test off 6500 hours | | |

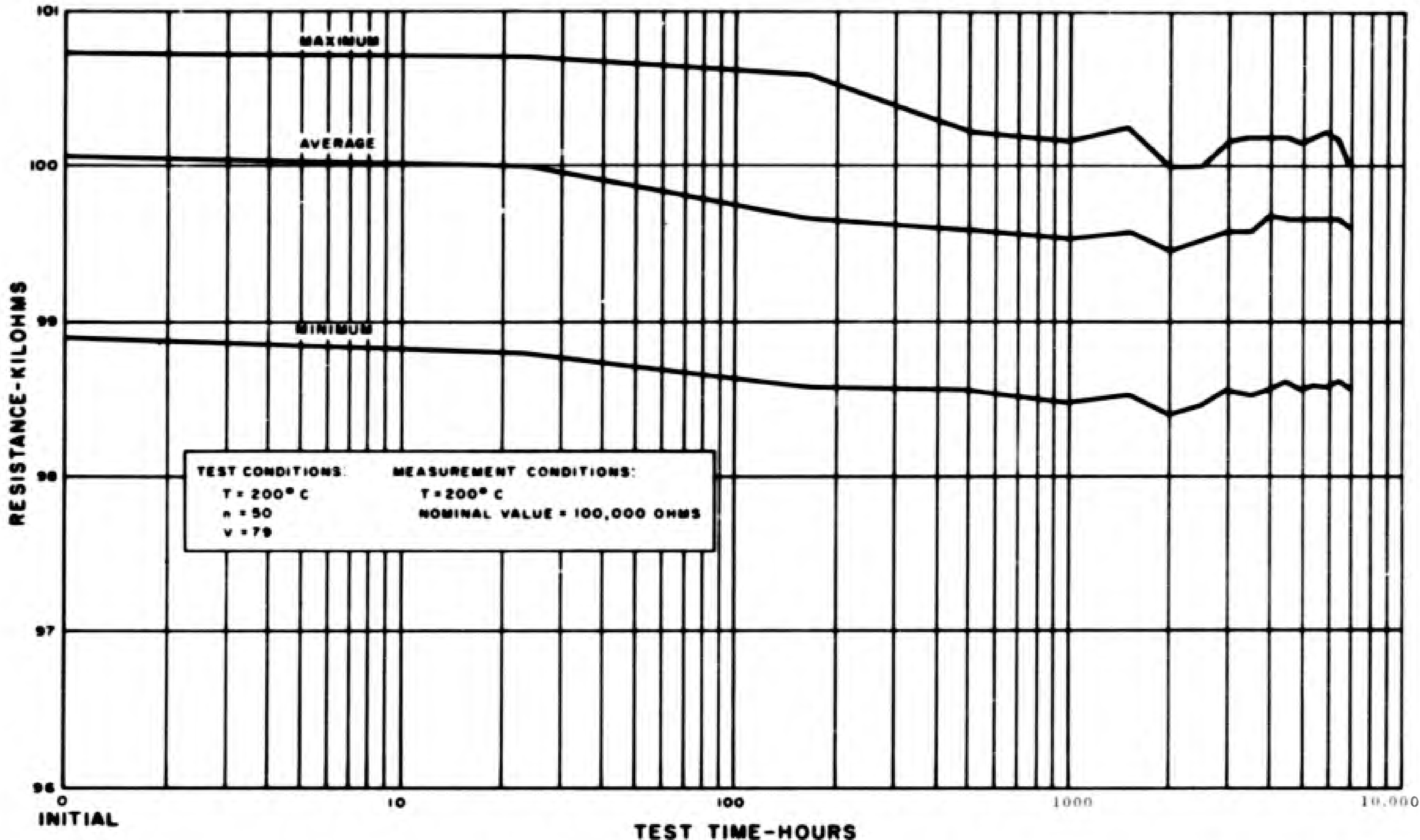


Figure 2-4. R2016P1003 - Phase IV - Resistance Variations

On the average the change in resistance slightly exceeds a negative 0.5 percent at 2000 hours. The resistance increased slightly during the next 5000 hours. The greatest negative change observed for a single resistor was 1.5 percent at 2000 hours.

The resistors on Phase V (150°C), Phase VI (50°C) and ambient life (25°C) have shown smaller changes in resistance than those noted above. This is as expected since the temperature of the active elements is the stress which produces the changes in resistance.

### 2.7.2 Capacitors

The Advent data, including the data accumulated following the Advent final report, have been processed by computer. The print-out shows a matrix of the input capacitance and dissipation factor values; matrix of delta values for each time interval; matrix of sums of delta values; and the maximum, minimum, average and standard deviation of each of the above for each time interval.

The analysis of the capacitor data will be based on the Eyring relation (Sec. 2.3.1), repeated here for convenience.

$$R = a_1 T^W e^{-\frac{b}{KT}} e^{S\left(c + \frac{d}{KT}\right)}$$

It is assumed that the rate of degradation is proportional to the rate of the chemical reaction governing the dominant failure mechanism. It has been generally observed for dielectric materials that the stress can be expressed as the logarithm of voltage at constant temperature. Thus,

$$R = R_o e^{\ln V^n} = R_o V^n = k \frac{dD}{dt} \tag{26}$$

where k is the constant of proportionality.

Or, rearranging terms of Equation (26), we have

$$dD = \frac{R_o}{k} V^n \; dt \tag{27}$$

$$D = \frac{R_o}{k} V^n t + c = G V^n t + c \tag{28}$$

where

$$G = \frac{R_o}{k} \text{ and } c = D_o = \text{state of damage at } t = 0.$$

D might represent an intrinsic characteristic of a part or material, as intrinsic dielectric strength. $D_o$ would be a variable representing the departure from the ideal condition due to manufacturing variations, handling, etc.

For dielectric type capacitors the measurable part parameters usually show little change until just prior to catastrophic failure. The results will, therefore, be plotted for catastrophic failure only.

A plot of the failure data for paper-plastic capacitors, the commercial prototype of the R2022 part, gave a straight line between log voltage and log time in agreement with Equation (28) (Advent Report). The slope of the line gave a value of 10 for n. Knowing n the relative damage at each step of the step-stress test can be calculated as $V^n$ t, from Equation 28, and summed to give the total damage.

Table 2-5 gives the results of this calculation for the Phase I, II, and III tests on paper-plastic capacitors.

TABLE 2-5. EQUIVALENT DAMAGE PER UNIT TIME AT EACH STEP PAPER-PLASTIC CAPACITORS - PHASES I, II, AND III

| DIRECT VOLTAGE | $V^{10}$ | $\Sigma V^{10}$ |
|---|---|---|
| 1200 | $6.2 \times 10^{30}$ | $6.2 \times 10^{30}$ |
| 1300 | 13.8 | 20 |
| 1400 | 29 | 49 |
| 1500 | 58 | 107 |
| 1600 | 110 | 217 |
| 1700 | 200 | 417 |
| 1800 | 360 | 777 |
| 1900 | 610 | 1387 |
| 2000 | 1020 | 2407 |
| 2100 | 1660 | 4067 |
| 2200 | 2650 | 6717 |
| 2300 | 4200 | 10920 |
| 2400 | 6300 | 17220 |

The time required at a constant voltage stress to give the same damage as a step stress test can be easily calculated when the slope is known.

$$t_{\text{constant voltage}} = t_{\text{per step}} \frac{\Sigma V^n \text{ step voltage}}{V^n \text{ constant voltage}} \quad (29)$$

Failure mechanism studies are continuing on the glass capacitors in an attempt to determine the current conduction and failure mechanisms of the part. From the results of these investigations, accelerated tests designs will be generated which will accentuate the cause of failures at measurable rates. The above analyses will then be used.

### 2.7.3 Semiconductors

The accelerated step stress tests for the semiconductors during the Advent evaluation program provided one excellent example of the use of accelerated testing for determining long life capability of electronic parts. The analysis was performed using the method presented in Section 2.4 above on the R2008P5 diode.

The R2008P5 diode (1N751A) is a hermetically sealed, silicone, alloy junction, Zener-type voltage regulator, subminiature diode. The maximum rating is 400 milliwatts at 25°C ambient and 0 milliwatts at 175°C ambient. The nominal breakdown voltage is 5.1 volts at 25°C ambient. It is in a D0-7 (glass) case, dry-air filled.

A Phase I (24-hour steps) and a Phase II (120-hour steps) step stress test program was performed on samples of 50 each. Using the above mentioned analysis plan, a plot of junction temperature versus the normal probability scale was made and it is shown in Figure 2-5. Selecting the 1 percent and 50 percent failure points for each phase test, these points may be replotted on a junction temperature versus log time scale as shown in Figure 2-6. Linear extrapolation of the lines shows an expected 1 percent failure occurring at about 8000 hours.

Two high-level, constant-stress tests were also performed. A Phase IV test at 200°C ambient and a Phase V at 150°C ambient were run and failures were collected using the same definition of failure as the step stress tests. By determining the junction temperature of each diode through the use of individually measured thermal resistance values, a plot of junction temperature versus log time to failure was made as shown in Figure 2-6. This chart shows a life expectancy of 2 percent failures occurring at about 6000 hours of life at 25°C. The ambient life tests (25°C) failures are plotted on the same chart and show failures occurring at 4000 hours.

A comparison of the slopes of the lines from the two figures shows that they are parallel and it may be inferred that the same failure mechanism is operating in each case.

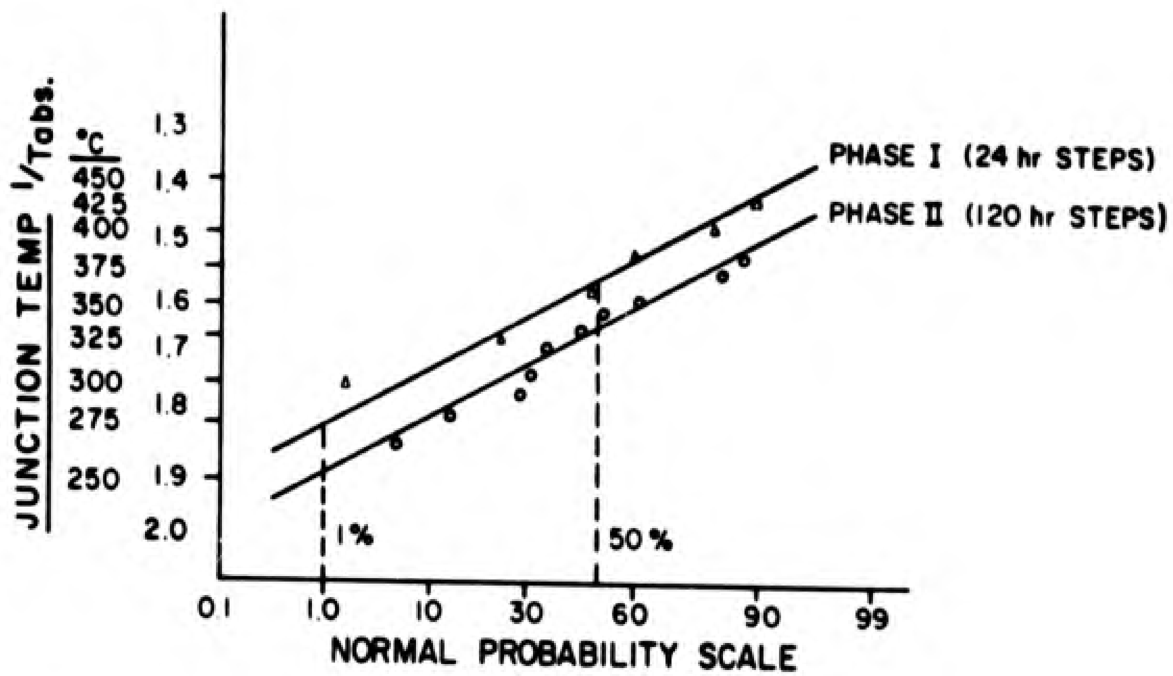


Figure 2-5. R2008P5 Failure Pattern

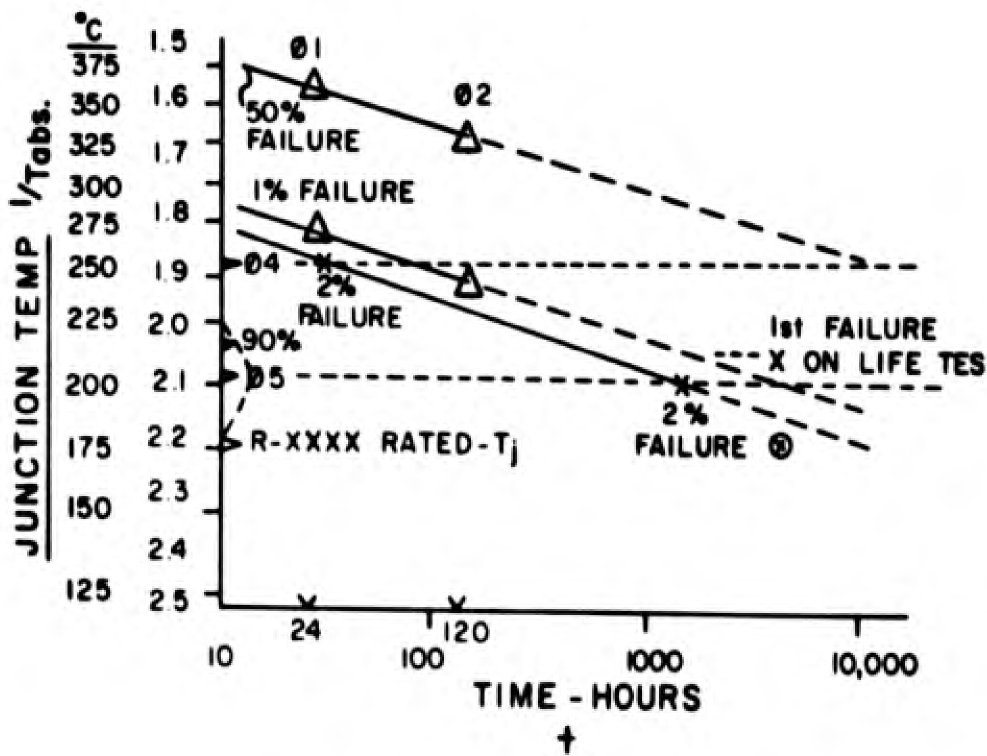


Figure 2-6. R2008P10 Design Data Chart

The inaccuracy of the predicted time to 2 percent failure between the accelerated tests and the rated tests used could be due to a number of physical factors and be further clouded by the small sample size. However, for use in determining the capability of the part to perform for a 50,000-hour mission at the given conditions, the accelerated tests were entirely satisfactory.

The failure mechanism which governed the useful life of this part was that of degradation of the epoxy mounting the die to the cathode lead. Severe derating of this and similar parts to 25 milliwatts would provide the required lifetime but would not be satisfactory for the power requirements of the vehicle design.

During the Advent data review on semiconductors, various observations were made on the behavior of devices on step and constant stress tests. A tentative qualitative model to rationalize the observed behavior during failure analyses was developed, and the development and set-up of detailed investigations were initiated.

Observations

1. Those diodes under ac operating stress conditions are exhibiting little or no change in monitored parameters compared with the continuously reverse biased R2008P10.

2. Step stress and constant stress data for the R2008P10 (1N758) exhibited a qualitative correlation to approximately the 200°C step. For thermal steps above 200°C, reverse current, which had been increasing, decreased to near initial values.

3. The drift mode behavior of transistors on constant stress tests possesses a net trend toward that associated with surface related phenomena.

4. A large number of transistor failing by $h_{FE}$ and $I_{CBO}$ have essentially recovered after a short 300°C bake; in more severe cases, a mineral acid (strong polar solvent) treatment of the surface has been required to produce recovery.

5. The behavior of transistors type R2026 (2N708) is shown in Figure 2-7. During the nine month shutdown the leakage current decreased by a factor of five. On reapplication of voltage the rate of change of $I_{CBO}$ has been almost the same as it was originally.

6. The R2008P10 Phase IV (200°C) failures all exhibited evidence of melting, primarily by the presence of gold-silicon solidified globules and ohmic electrical characteristics. A check of junction-to-case thermal resistance of unfailed devices indicated an increase of about 50 percent.

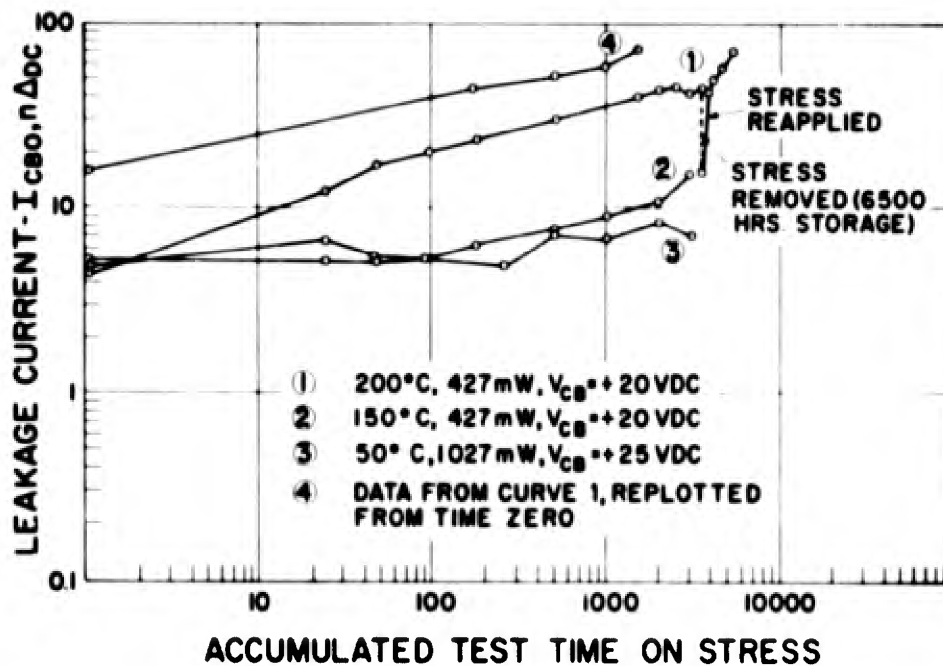


Figure 2-7. Leakage Current as a Function of Time

Discussion

Observation number six is probably directly related to a change in processing which this vendor recently introduced. A relatively high frequency of particles consisting of gold-epoxy occurred in these devices. The source of these flakes was the baked gold-epoxy die support material; specifically, many of the particles appeared to be derived from a thin strip of this material which wetted the edges of the die during dipping. Three hypotheses were advanced by the vendor to explain the phenomenon; these were diffusion of copper from the dumet-lead into the gold-epoxy and resultant decrease in its adhesive properties; the high specific gravity of the gold; and the tendency of the fine gold particles to agglomerate during the baking process. This phenomenon was apparently effectively eliminated by nickel plating the cathode lead "post" and by using silver powder with a substantially reduced tendency to agglomerate.

The observations one through five are believed to be relatable to a surface contaminant model, at least similar to the Atalla model. For observation one, a continuous field under reverse bias should accelerate charge collection and maintenance as compared with the ac conditions which produce a small field polarity reversal.

The reverse current recovery of the R2008P10 for temperature steps above 200°C suggests charges leaving the surface. Observation three is as stated and observations four and five are both compatible with surface behavior models.

The memory phenomena widely reported for semiconductor surface effects appears to be separated into two segments. Figure 2-7 shows a residual increase in leakage current after 6500 hours of storage. This residual represents a deterioration effect which might be equated with memory. The slope of the log leakage current - log time curve (Curves No. 1 and No. 4) shown in Figure 2-7 are similar, which indicates the mechanism of deterioration and its time dependence has not changed, nor has a "memory" been exhibited. Plotting total accumulated bias time without regard for the interruption of the test shows an apparent "memory" in that a high initial slope is obtained. In this case, this only represents the manner in which time is accumulated, and plotted and not a physical behavior pattern as such. Therefore, it would appear more logical to plot log current versus log time only for increments of time during which junction bias has been continuously applied.

# 3. FAILURE MECHANISM STUDIES

The physics of failure studies being conducted as a part of this program have the following goals:

1. To determine the "life" limiting failure mechanisms of high reliability R series resistors, capacitors, transistors and diodes,

2. To evaluate the part operating parameters which are sensitive indicators of these mechanisms, and

3. To evaluate the stress and stress levels which are valid in accelerating the failure mechanisms.

## 3.1 RESISTORS

### 3.1.1 Metal Film Resistors

A method has been derived which will provide the means to plot resistance change versus combined time and temperature values on a single chart. The derivation and limitations of this parameter $\theta$, are discussed in Appendix I and the form of the parameter is as follows:

$$\theta = T (15 + \log t) \times 10^{-3}$$

where

T is temperature in degrees Rankine

t is exposure time in hours.

For step-stress tests the accumulated time-temperature exposure was calculated by reducing each step to an equivalent time at a reference temperature, as follows:

$$T_T (15 + \log t_T) = T_R (15 + \log t_R)$$

where subscripts T represent test values for individual steps and subscripts R represent values at a reference temperature. Then:

$$\log t_R = \frac{T_T}{T_R} (15 + \log t_T) - 15$$

And the cumulative time-temperature exposure for the step stress tests is calculated using the sum of the equivalent times at the reference temperature:

$$\theta = T_R (15 + \log \Sigma t_R) \times 10^{-3}$$

The constant in the relationship is equivalent to the logarithm of the frequency factor A in the Arrhenius expression:

$$K = Ae^{-Q/RT}$$

where

Q is the activation energy

R is the gas constant

T is the temperature

K is the reaction rate constant

Resistance change values for all tests are plotted for 10,000, 20,000 and 100,000 ohm resistors in Figures 3-1 through 3-3 as a function of the time-temperature test exposure parameter, when temperature is expressed in degrees Rankine and time in hours.

Note that the resistance change values for all tests form a pattern, showing good correlation and continuity. This indicates that the time-temperature parameter plot is a useful method of comparing data from widely divergent test exposures including step-stress and constant stress.

The general shape of the curves for each value of resistor is the same. That is, resistance first decreases and then increases. This indicates the presence of at least two mechanisms of resistance change. The initial downward drift probably represents stress relief, as discussed by several authors*. The maximum negative drift observed occurred in the 10,000 ohm resistors. A lesser degree of negative resistance drift was observed in the 20,000 ohm resistors and still less was observed in the 100,000 ohm resistor. The film thickness decreases as film resistance increases, and since the ratio of area to volume increases as the film becomes thinner, the

---

*Bretts, G.; Kozol, J.; and Lampert, H., "Failure Physics and Accelerated Testing", Vol. 2 Physics of Failure in Electronics, RADC Reliability Series, 1964, p. 189.
McDonald, W. J., "The Effect of Heat Treatment in Preparing Metal Films for High Temperature Service", WADC TR 58-468, 1958.
Olson, E. R. and Vajda, G. V., "Physics of Thin Resistive Films", Halex Corp. Progress Report No. 1 to WADC, Sept. 1959.

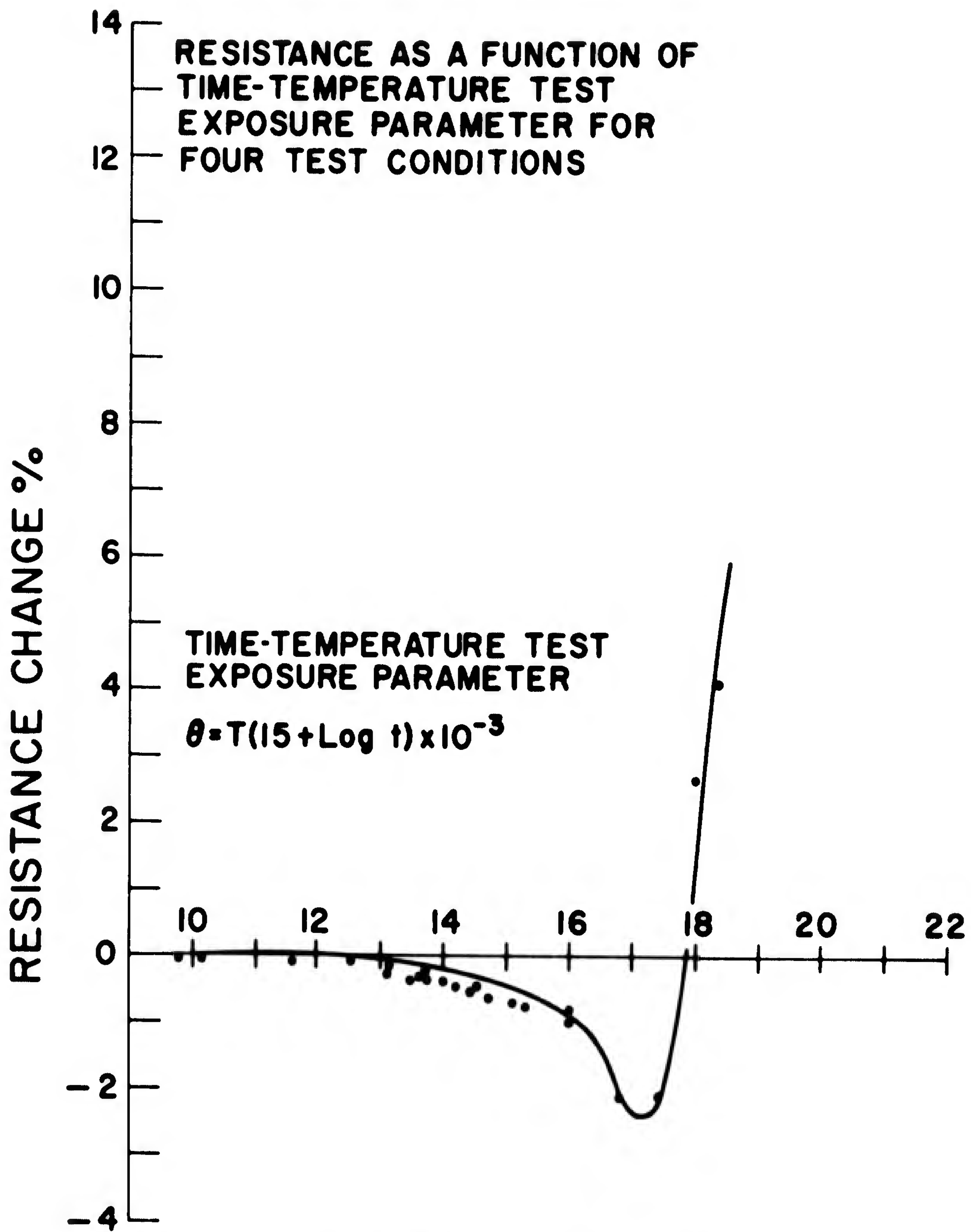


Figure 3-1. 10,000 Ohm Metal Film Resistor - Resistance Change

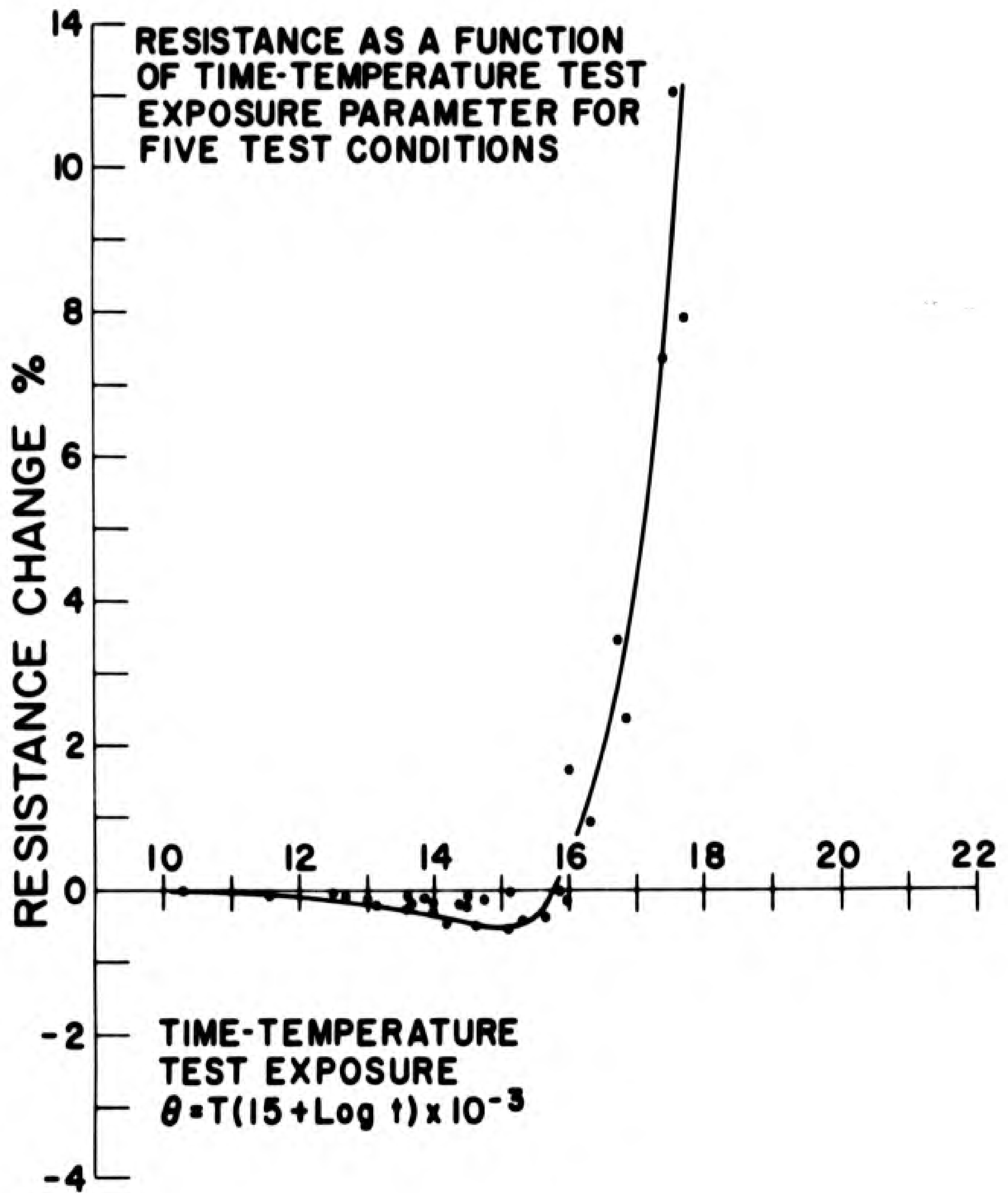


Figure 3-2. 20,000 Ohm Metal Film Resistor - Resistance Change

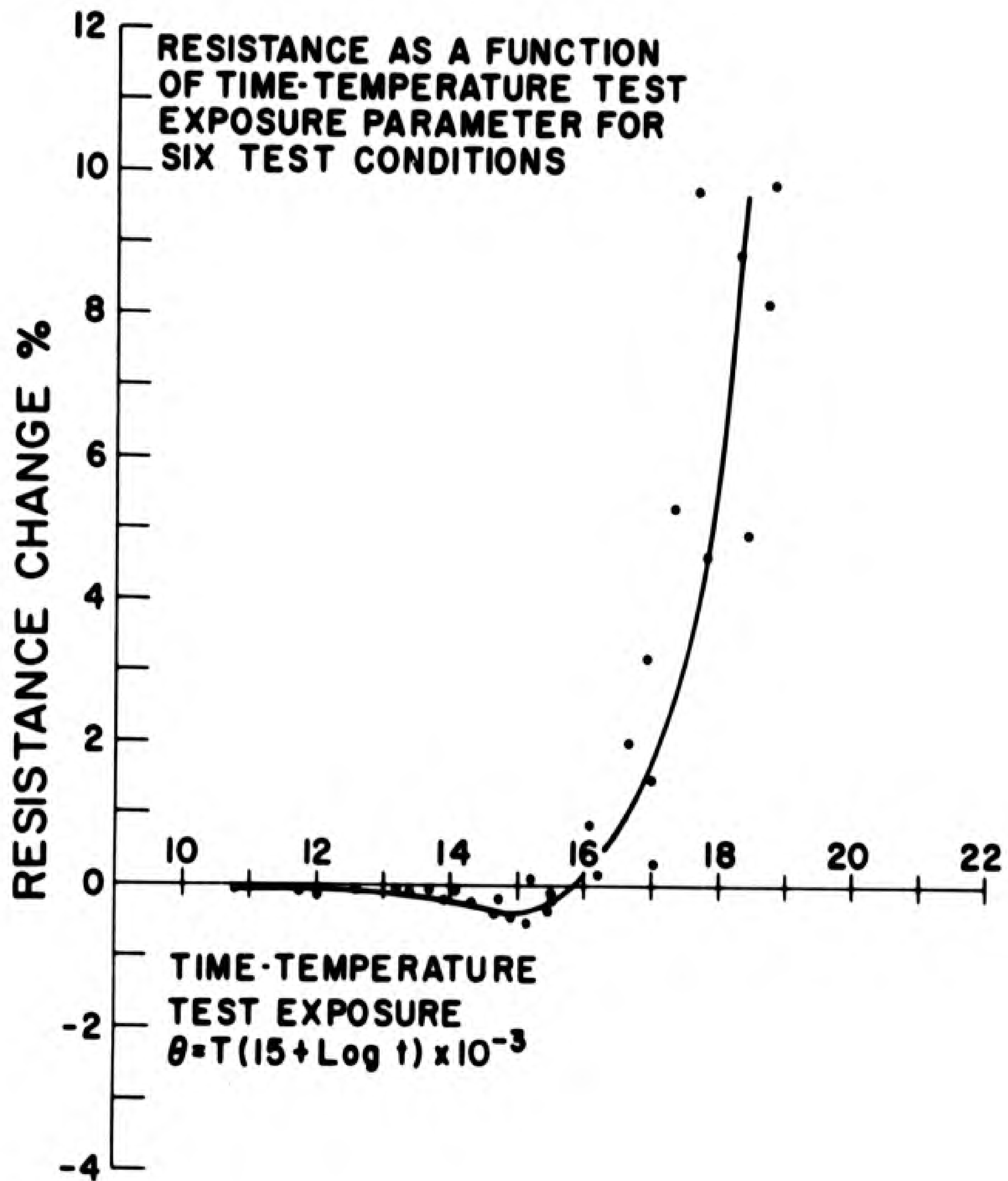


Figure 3-3. 100,000 Ohm Metal Film Resistor - Resistance Change

observation is that which would be expected. In addition, the time-temperature exposure at which maximum negative drift is observed decreases as resistance increases. The oxygen diffusion path length decreases such that the onset of oxidation effects is observed sooner in thinner films.

Figure 3-4 shows a plot of cumulative absolute resistance change values from the 100,000 ohm metal film resistor tests as a function of the time temperature parameter.

The activation energy calculated is close to that which might be expected for a reaction controlled by interstitial oxygen diffusion. The theoretical value of the frequency factor A for oxygen diffusion in nickel is 17 which is close to the value of 15 selected for the parametric constant. The reaction which appears to govern positive drift, then, is an internal oxidation and precipitation reaction. This would appear to be reasonable since it is not obvious that oxygen or other diffusing interstitial elements are available in large excess in the part package.

### 3.1.2 Oxide Film Resistors

Doped tin oxide films have been found to drift as a result of diffusion dependent phenomena. Tests similar to those reported for metal films were conducted on tin oxide film resistors.

Resistance change values for 100,000 ohm oxide film resistors are plotted as a function of time-temperature test exposure parameter in Figure 3-5.

The resistance change values for all tests again show a good pattern, with good continuity between constant stress and step stress tests. The time-temperature parameter again provides a useful tool for comparing results from varying tests.

The shape of the curve is of considerable interest. Three general areas are evident, first an increasing resistance with time and temperature, second, a rapidly decreasing resistance, and third, a rapidly increasing resistance. The rapid decrease in resistance is the result of the dissociation of stannous oxide into stannic oxide and tin which takes place above 385°C.* It has been emphasized that accelerated test data must be representative of normal conditions. It is apparent from Figure 3-5 that several things have happened in the course of testing. All points which represent resistance decreases were taken at temperatures over 350°C. The data in this regime are the result of a new mechanism which is not related to the mechanism operative at lower temperatures.

*Middleton, A. R. and Herczog, A., "Ultra High Temperature Oxide Fixed Film Resistors", WADC TR 58-468, 1958.

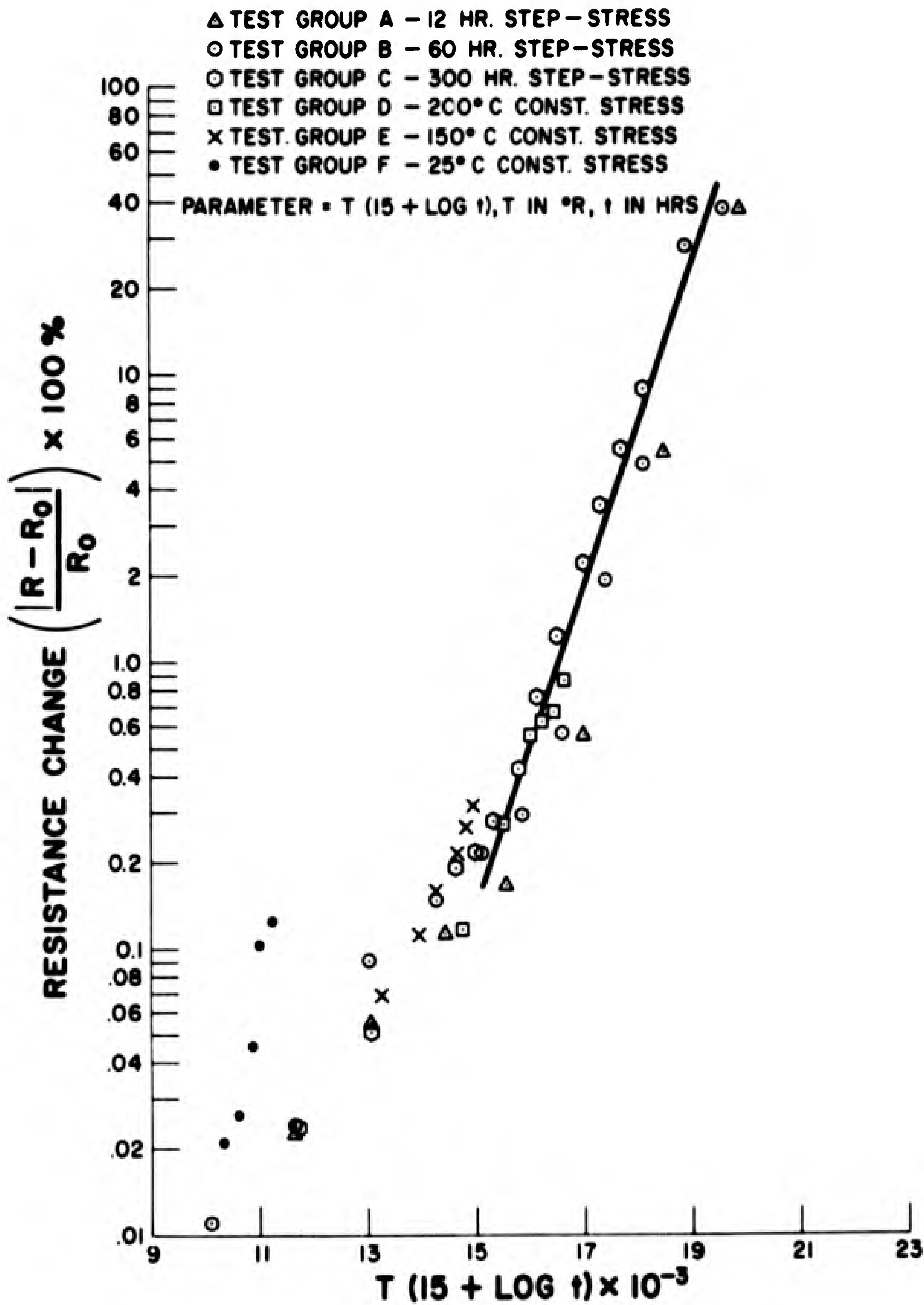


Figure 3-4. Absolute Resistance Change as a Function of Time-Temperature Parameter for 100,000 Ohm Metal Film Resistor

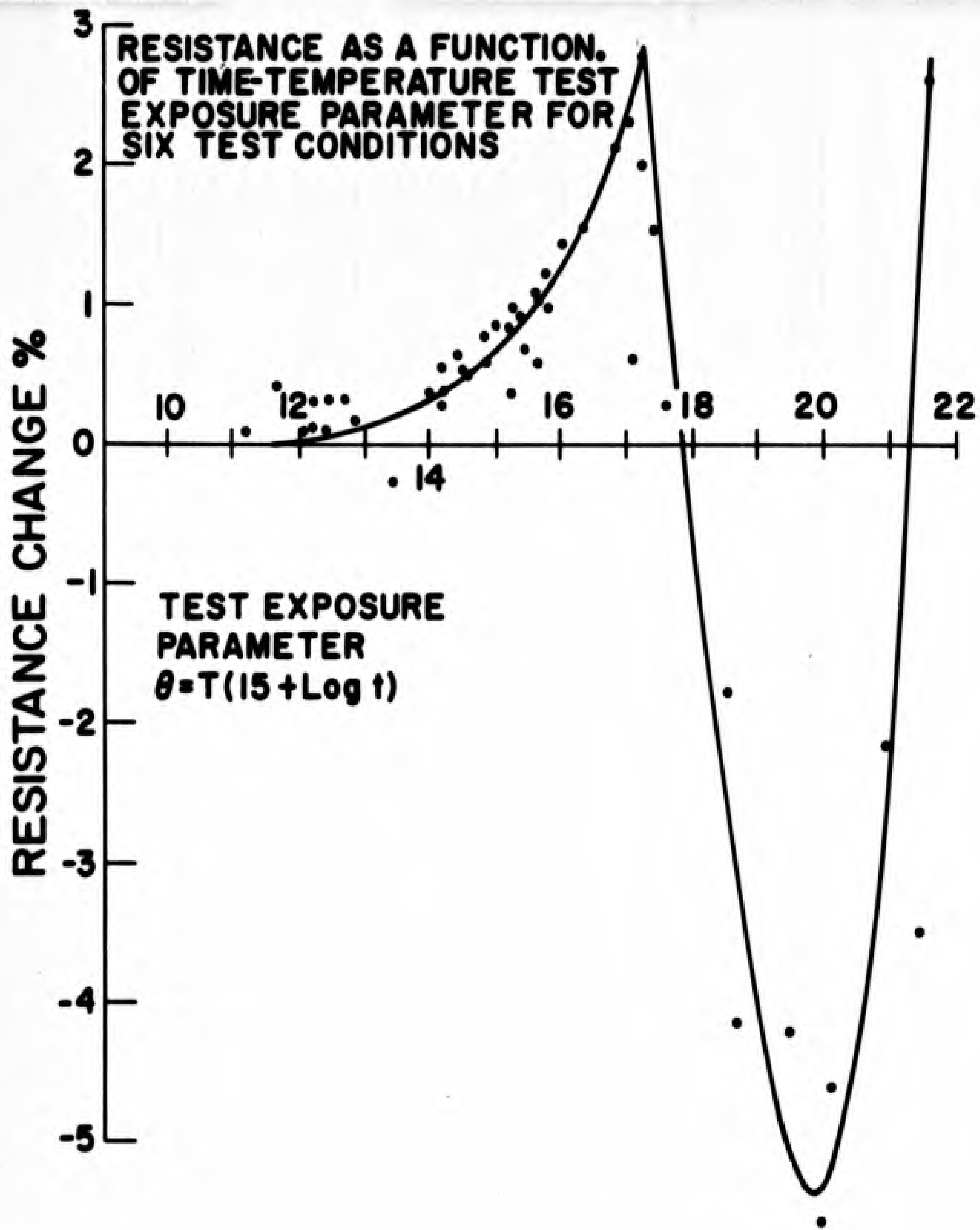


Figure 3-5. 100,000 Ohm Oxide Film Resistor - Resistance Change

BLANK PAGE

The activation energy for the process operating at temperatures below the onset of the stannous oxide decomposition was determined in the manner described previously. The activation energies determined from plots of 1/T versus log t at 5, 2, 1, 0.5, 0.2 percent and 0.1 percent damage were 33.8, 33.9, 32.1, 36.3, 37.5 and 35.6 K cal respectively. The upward drift in resistance therefore probably results from a diffusion dependent reaction having an activation energy of 35 K cal.

Figure 3-6 shows a plot of cumulative absolute resistance change as a function of the time-temperature parameter. The deviations from linearity at the upper end of the curve represent values taken above 350°C which are not representative of the dominant mechanism under study. The activation energy calculated in this case is more nearly representative of self diffusion process such as tin in tin or tin oxide than an interstitial process.

## 3.2 CAPACITORS

### 3.2.1 Glass Capacitor

In contrast to the extensive aging mechanism information available on metal film resistors, glass dielectric capacitors have relatively little information published. A published work which established that voltage step stressing of mica capacitors correlated with constant stress results has provided useful data.* Since it followed from these results that a voltage-time dependent polarization mechanism preceded failure in this mineral dielectric, it was considered that similar results might be expected in the glass dielectric.

A schematic illustration of the glass dielectric capacitor is shown in Figure 3-7. The dielectric material is a potash-lead glass. Chemical analysis of a typical sample provided the composition shown in Table 3-1.

During the Advent Parts Testing Program series of voltage step stress tests, with increasingly longer steps, resulted in observations contrary to those expected. The devices subjected to the longer steps failed (by dielectric breakdown) at higher voltages than did those subjected to shorter time steps.

Physical analysis of the failures from the complete group of tests revealed that the lower voltage and shorter time failures were concentrated at the ends of the foil plates of the capacitor. The higher voltage failures occurred between the plates and away from the end edges as shown in Figure 3-8. The correlation of voltage-time to failure and failure location was very good.

---

*Endicott, H. S. and Zoellner, J. A., "A Preliminary Investigation of the Steady and Progressive Stress Testing of Mica Capacitors", Proc. Seventh National Symposium on Reliability and Quality Control, Jan. 9-11, 1960, p. 229-235.

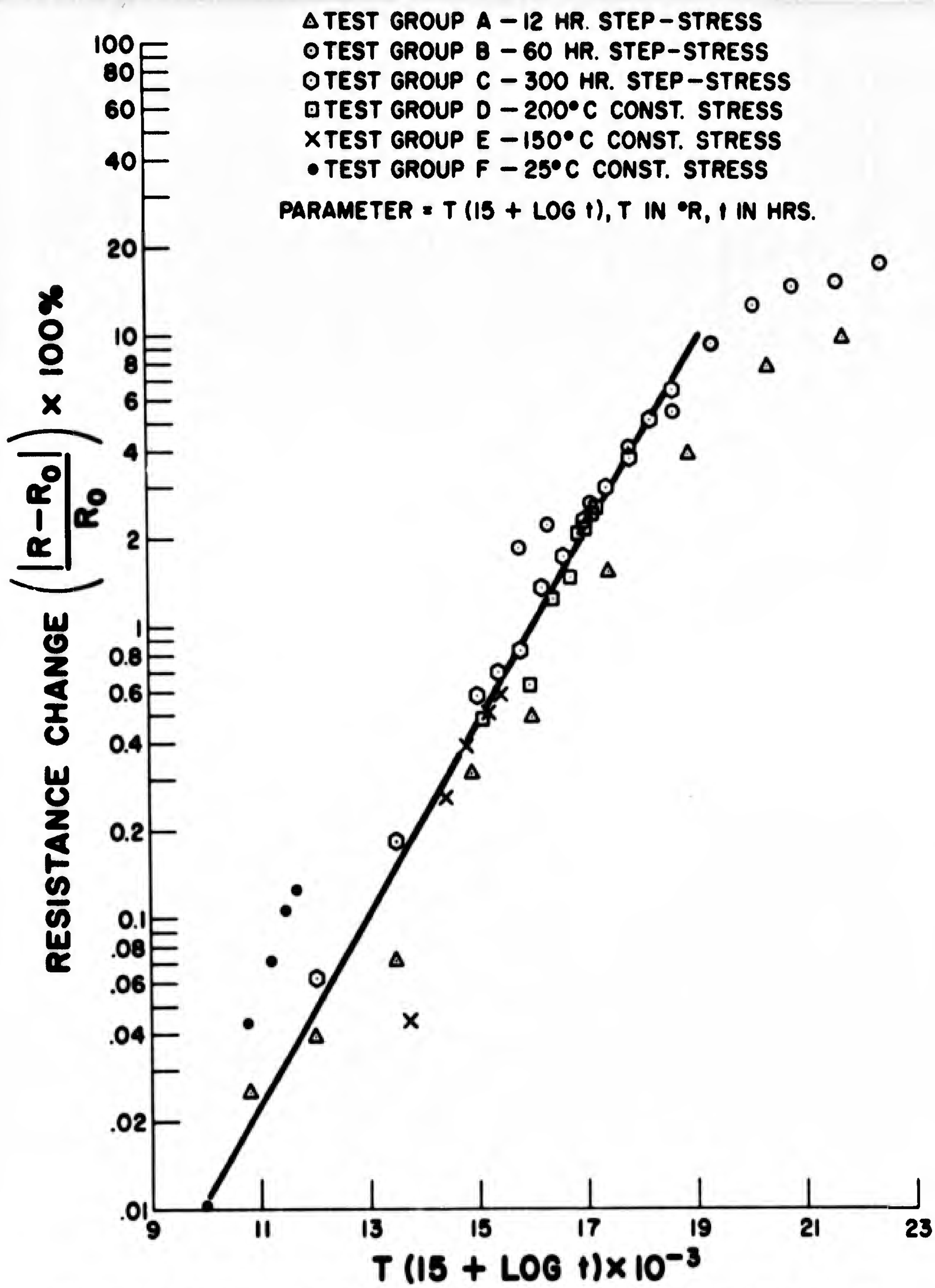


Figure 3-6. Absolute Resistance Change as a Function of Time-Temperature Parameter for 100,000 Ohm Oxide Film Resistor

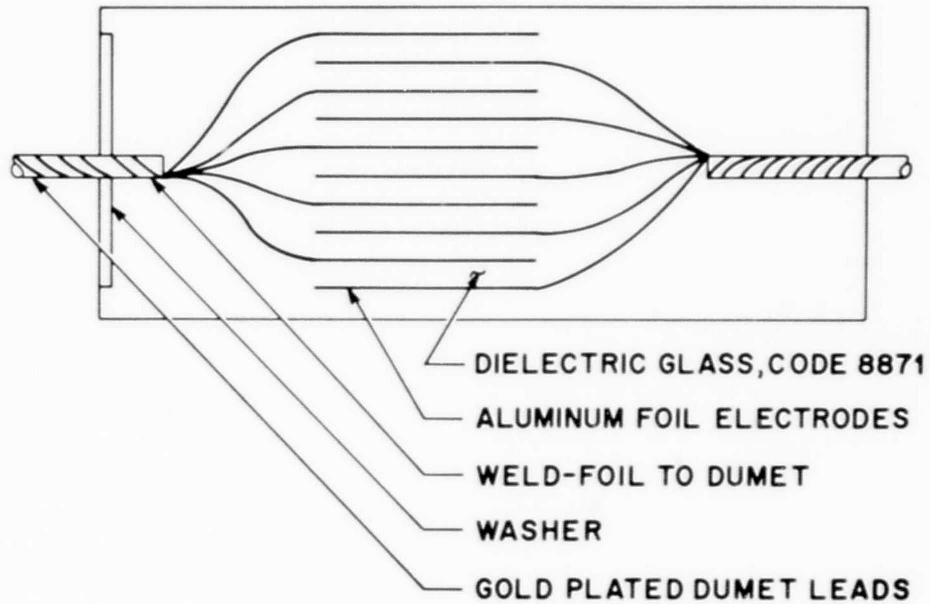


Figure 3-7. Glass Capacitor

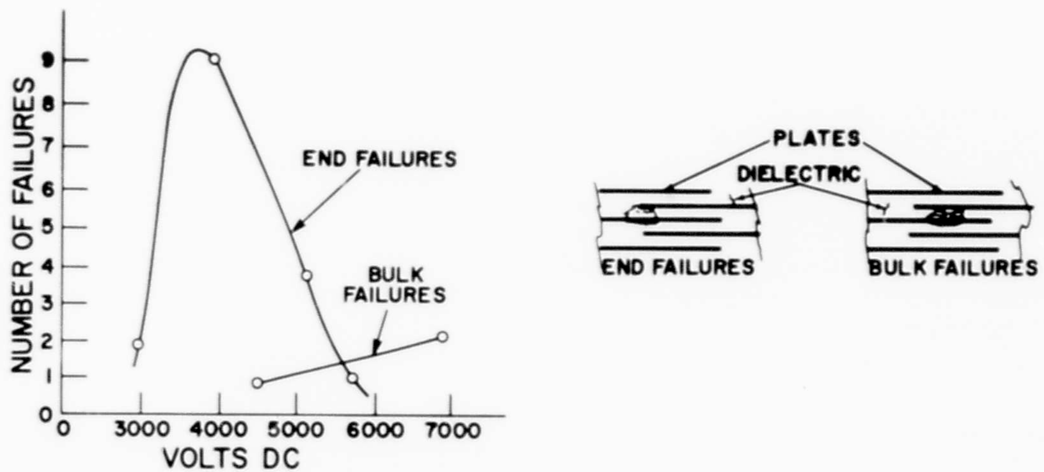


Figure 3-8. Glass Capacitor Failure Distribution

TABLE 3-1. CHEMICAL ANALYSIS OF CAPACITOR GLASS

| CONSTITUENT | REPORTED AS | WEIGHT CONTENT, % |
|---|---|---|
| Silicon | $SiO_2$ | 40.02 |
| Lead | PbO | 44.75 |
| Antimony | $Sb_2O_3$ | 1.70 |
| Tin | $SnO_2$ | 0.65 |
| Bismuth | $Bi_2O_3$ | 0.39 |
| (1) | Oxides | 0.42 |
| (2) | $R_2O_3$ | 0.71 |
| (3) | Oxides | 0.16 |
| Sodium | $Na_2O$ | 3.82 |
| Potassium | $K_2O$ | 5.80 |
| Boron | $B_2O_3$ | Present, Not Determined |

(1) Ammonium Sulfide Group. Vanadium, Manganese, Cobalt, Nickel, Zinc, Tungsten, Titanium.

(2) Ammonium Hydrozide Group. Beryllium, Aluminum, Phosphorus, Selenium, Chromium, Iron, Gallium, etc.

(3) Ammonium Oxalate Group. Calcium, Strontium, Barium.

The location of failure as a function of voltage alone is not particularly striking, since one would expect that the concentration of voids, defects and geometrical variations would be very highly concentrated at the foil ends. The point that is of interest however, is that the distribution of failure location changed almost completely with lower voltage-time bias history. That is, almost all failures on short time-voltage step stress (30 minutes, 100 volt increments) were concentrated at the foil ends at a voltage of roughly 4500 volts while failures in longer time-voltage step stress (5 hours, 50 volt increments) shifted to the center of the foil and occurred at roughly 6000 volts.

To account for this behavior, it was hypothesized that the electrical field was reduced at the edge of the plates with increasing voltage-time bias so that the high gradient naturally present at the edge of a capacitor plate no longer exceeded that between the plates. The mechanism causing this change was postulated to be alkali ion migration in the glass network.

Work as early as 1884 had provided strong evidence for an electrolytic component of conductivity in glass*. The experimental evidence consisted of filling glass test tubes with mercury and with sodium amalgam and immersing the tube in a similar bath. The mercury and the amalgam served as electrodes for electrolysis studies on the glass. Tests with mercury electrodes demonstrated that conductivity rapidly diminished as electrolysis continued. This decline was ascribed to depletion of sodium ion current carriers at the anode. Tests with sodium amalgams demonstrated that no decline in conductivity of the glass with time occurred. Subsequent work** with potassium amalgam electrodes demonstrated that these ions would not replace the sodium in the glass. Lithium amalgams demonstrated conductivity, but the glass became opaque and embrittled. This work strengthened the theory of the mechanism of ionic conductivity in glass and demonstrated a dependence on ion size.

The mechanism of failure in glass capacitors is therefore believed to be related to the effects of sodium ion migration in this glass. Qualitatively it was felt that the sodium ions drifted toward the cathode plate under electrical stress, and formed a space charge region next to the electrode. This space charge region followed the contour of the electrode on a microscopic scale and hence caused a highly uniform field to be developed near the plate rather than a non-uniform one as had previously existed.

A mathematical analysis of the distribution of sodium ions at equilibrium with a uniform electrical field in an ideal glass capacitor was accomplished. The model of the system is a dielectric of thickness L and dielectric constant D which contains mobile positive ions whose concentration $\rho^+$ is a function of the distance x in an applied field, and immobile negative ions whose concentration $\rho^-$ is independent of x. Based on the electrochemical potential of positive ions, Poisson's equation, and assuming the net charge in any region is small compared with either the total negative or positive ion concentrations, the net charge distribution becomes:

$$g = -\frac{VC\,K'}{8\pi}\;\frac{\sinh\sqrt{C}x}{\sinh\sqrt{C}L/2}$$

where g is defined as $\rho^+ - \rho^-$

$$C = \frac{4\,Z\pi\rho^-\,e.}{K'RT}$$

V = Voltage

K' = Dielectric Constant

L = Dielectric Thickness

*Warburg, E., "The Electrolytic Conductivity of Glass", Ann. Physik-Chem., 21, 622 (1884).

**Tegetmeier, F., Ann. Physik-Chem., 41, 18, (1890).

Z = Degree of Ionization

$\rho^+$ = Positive Ion Concentration

$\rho^-$ = Negative Ion Concentration

e = Electronic Charge

R = Gas Constant

T = Absolute Temperature

The derivation of the equation is given in Appendix II. Additional calculations are shown in Appendices III and IV. Graphically, the equilibrium condition is shown in Figure 3-9.

In this illustration, (a) represents the shape of the energy bands due to the application of the voltage V. (b) is the charge distribution at equilibrium resulting from the applied voltage V. (c) shows the position of the conduction and valence energy bands of electrons resulting from the charge distribution shown in (b). The net position of the energy bands is obtained by algebraically summing (a) and (c). From measurements of the ultra-violet edge of the absorption region of the dielectric glass, the forbidden energy gap has been calculated to be approximately four electron volts. Should the

## ENERGY BANDS AND ION DISTRIBUTION

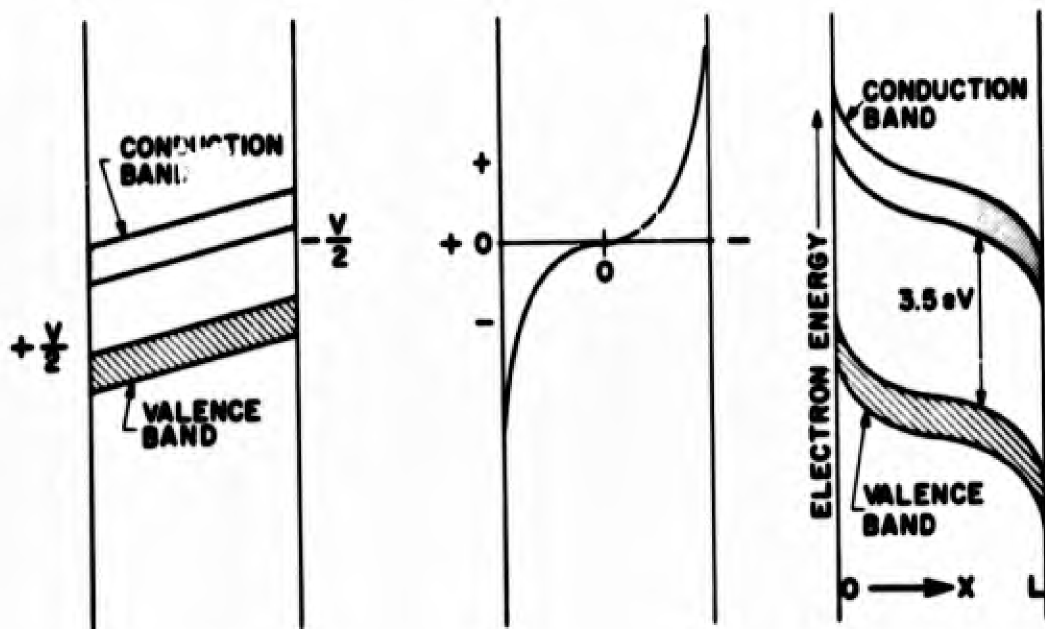


Figure 3-9. Energy Bands and Ion Distribution

configuration of the energy band gap be modified sufficiently by the calculated final ion distribution, either thermionic emission or quantum mechanical tunnelling can occur. This would give rise to sufficient joule heating to permit exponential current increase and catastrophic failure.

Concurrently with this analysis of equilibrium conditions, analysis is being made of the dynamic processes which would account for the observed experimental behavior. To this end, a study of the charging current for these capacitors is in progress extending from the time of voltage turn-on through most of the absorption current region to times in excess of $10^5$ seconds.

While the equilibrium conditions were the most accessible for modelling, it was recognized that these may not predict a failure mechanism that is active within device rating. Since various transients and changes in applied voltage levels are to be expected in d-c applications, an equilibrium analysis only partially reflected application conditions. In addition, though failures were anticipated, it was found that square wave pulsing (one second off-one second on) at approximately 50 percent of short-time dielectric breakdown voltages, produced failures within about 100 pulses. The distribution of failure was bi-modal and apparently temperature independent, though also highly dependent on circuit series resistance (the charging time constant).

The pulse condition behavior was interpreted to mean that transient phenomena should not be neglected in modelling for failure. For instance, the large and extended decay time polarization current suggests that the d-c dielectric constant may be much larger than the value at several megacycles. In that case, the potential gradient within the dielectric inducing the ion transport or electronic phenomena should be correspondingly larger at voltage turn-on or positive transient pulses.

As the first step in assessing non-equilibrium conditions within the dielectric, measurements of the absorption current were taken at various voltages and temperatures. These measurements were extended in time in order to simultaneously establish leakage current values. It is anticipated that establishing the functional dependency of leakage current on voltage and temperature could aid in validating the equilibrium model if a functional relation can then be found between the equilibrium model and leakage current values.

Adsorption current measurements planned for 20, 100, and 500 volts at 100°, 150°, and 225°C, are nearly completed. A description of the equipment and procedures used are nearly completed. A description of the equipment and procedures used are contained in Appendix VI. It is anticipated that the complete results and their analysis will be available for the next interim report.

Leakage current values obtained at 150° and 225°C are graphed as ln I versus ln V in Figure 3-10 and 3-11. It is to be observed that an excellent linear fit is obtained at 225°C where all measurements were taken on a single capacitor, serial number CB0039.

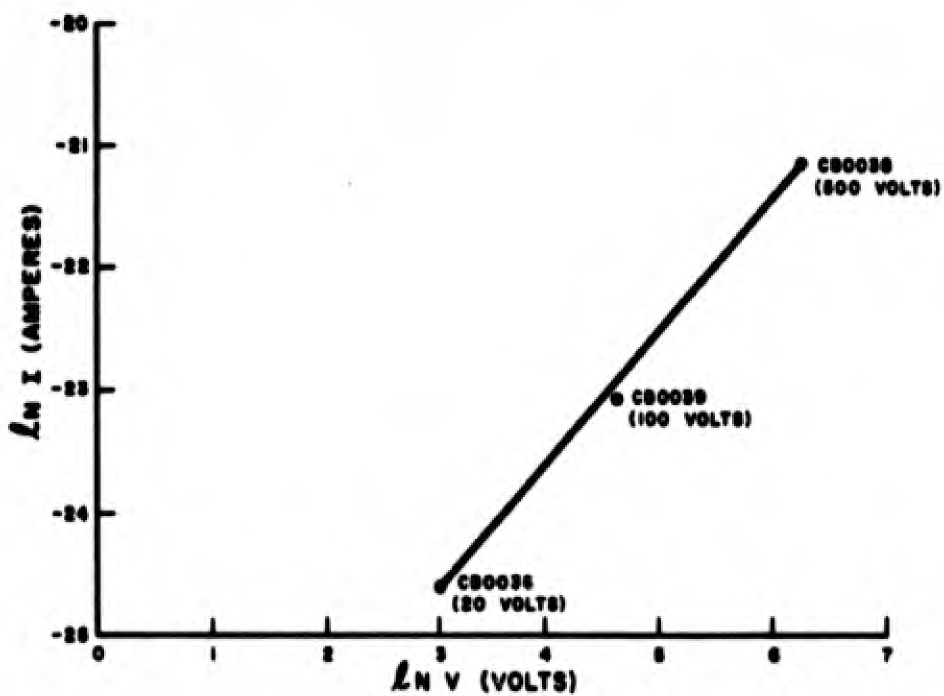


Figure 3-10. Leakage Current Versus Applied Voltages at 150°C

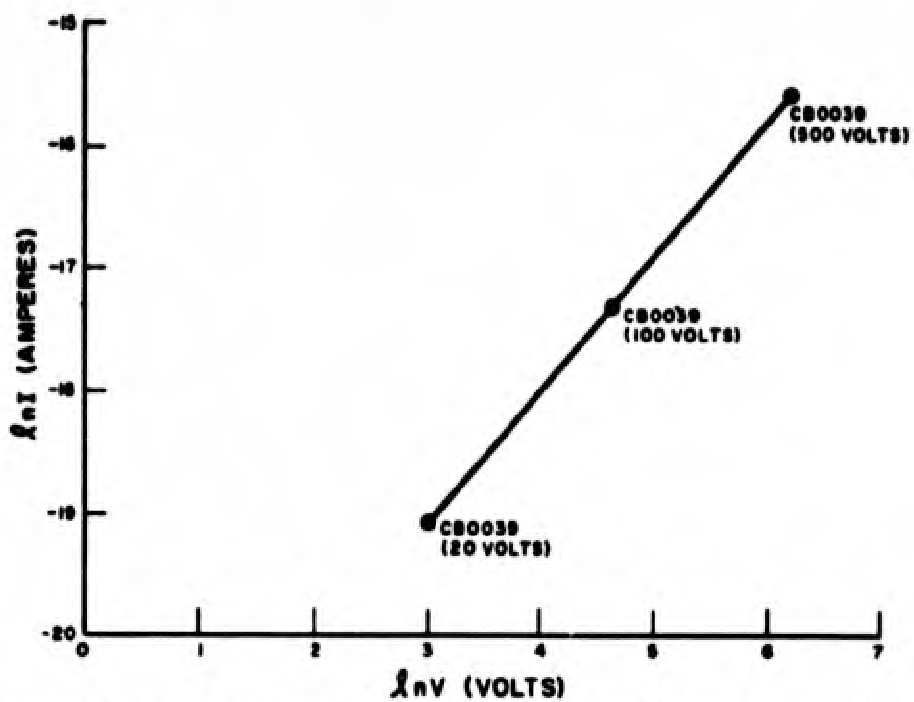


Figure 3-11. Leakage Current Versus Applied Voltages at 225°C

At 150°C it is not unexpected that the central point from CB0039 is to one side of a straight line between the end-points taken on CB0038. However, the slopes of the lines calculated from the actual end point measured values are in very close agreement. The calculated values are 1.099 (225°C) and 1.082 (150°C).

If possible, the values of leakage current at 100°C will be estimated from absorption current readings taken to times as great as ninety-six hours. A very tentative form of the total expression for leakage current appears to be

$$I_L \propto F(T)\, e^{-q/KT}\, V^n$$

where

F(T) = a function of temperature

T = degrees Kelvin

q = electronic charge

k = Boltzman's constant

V = voltage

n = a constant

3.3 SEMICONDUCTORS

The mechanism studies performed on diodes is discussed is Paragraph 2.7.3.

The deterioration mechanisms anticipated for the planar transistors during accelerated testing were associated with surface phenomena. The deterioration mechanism observed and reported during long-term tests under bias is the surface inversion layer or channel described by other investigators. *

---

*Peck, D.S., Blair, R.R., Brown, W.L., and Smits, F.M., "Surface Effects of Radiation on Transistors," Bell System Technical Journal, Jan. 1963, p. 95.

Metz, E.D., "Silicon Transistor Failure Mechanisms Caused by Surface Charge Separation," Vol. 2. Physics of Failure in Electronics, Mar. 1964, p. 163-172.

Results of tests conducted during the Advent program indicated that typical surface-induced failures occurred within an upper limit bounded by 200°C under junction bias and power dissipation within ratings and are discussed in Paragraph 2.7.3 of this report.

Several observations are available which aid in classifying the contaminant. First, the contaminant shows sufficient activity at 300°C that devices are rapidly and substantially restored. Second, the leakage current in devices with the same history as above can be reduced by rinsing the die with a strong polar solvent such as a mineral acid. Nonpolar and weakly polar solvents such as Xylene and Acetone do not reduce the leakage current. Third, the contaminant is readily affected (ionized or polarized) by the field extending from the reverse biased junction. The inversion layer model requires the deposition of a charged ion or uncompensated dipole on the device surface.

The source of the contaminant must of necessity lie within the hermetically sealed transistor enclosure. It has generally been ascribed to an existing contaminant layer on the die surface. Examination of the materials in the transistor enclosure for possible sources of ionic or polar contaminants led to the conclusion that a source of polar contamination may be the electroless gold or electroless nickel plating commonly used on the header and cap. The electroless process deposits phosphides concurrently with the desired metal by the reaction

$$2Au^{+} + H_2PO_2^{-} + 2OH^{-} \longrightarrow 2Au + H_2PO_3^{-} + H_2O \ .$$

A mass spectrometer analyzer was utilized to determine the presence of contaminants from this source. Appreciable quantities of phosphorus and compounds $H_2PO_2$ and $H\ PO_3$ were found in the effluent gases of the R2005P1 transistors when heated to 100°C.

These compounds could act in the following manner to create an inversion layer as illustrated in Figure 3-12. At a given temperature, a partial pressure of the phosphorus compounds exists inside the transistor enclosure. The concentration of these compounds will be proportional to the temperature. On the silicon dioxide surface, a number of energy sites exist of both positive and negative sign in equal number. These sites are partially occupied by the polar molecules derived from the contaminating gas. Without the application of an external bias, there is no net dipole field resulting from these molecules. When bias is applied, the energy associated with each of these sites is changed, the positive sites having greater energy in an N type material, and the negative sites having decreased energy. This change would favor the retention of the dipoles aligned in the higher energy sites by increasing the binding energy, and reduce the binding energy in the other sites. As a result of this, a larger number of the molecules in the high energy sites would remain on the surface than those in the low energy sites. In this manner, a net dipole would develop on each side of the junction. The role of temperature in this mechanism would be to control

# INVERSION LAYER FORMATION

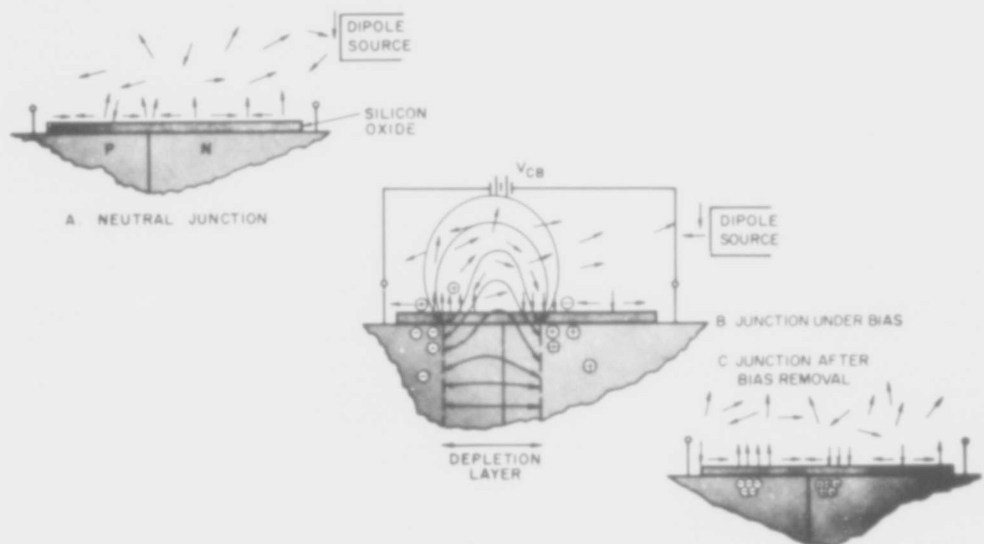


Figure 3-12. Inversion Layer Formation

the concentration of the contaminant in the gas phase, and hence the concentration in equilibrium with it on the surface. The energy of molecules on the surface would also be controlled by temperature. Upon removal of bias, the favored orientation of the molecules would not continue. This model would also account for memory with removal and reapplication of stress by having the contaminant simply adsorbed onto the transistor enclosure and therefore more rapidly desorbed than phosphides may be evolved from the gold.

There is no experimental evidence yet that these phosphorus compounds are actually present on the silica surface of an aged device because of the difficulty associated with its small size.

However, experiments are underway to determine the contribution of semiconductor temperature, junction bias, and source concentration by exposing planar devices to an atmosphere containing phosphides supplied by an external source.

BLANK PAGE

# 4. SPECIFICATION AND PROCUREMENT

## 4.1 GENERAL

The parts under evaluation for this program are General Electric R-Series, high reliability electronic parts procured for hardware use in the Advent Communication Satellite Program. The complexity of the Advent parts evaluation program was reduced by the selection of the minimum number of part types and kinds which would satisfy design engineering requirements. An Approved Parts List defined those parts which would be used for the spacecraft design.

It was recognized at the start of the program that parts specifications which were available to the industry were inadequate for assurance of long life in space vehicles. Procurement documents consisting of engineering specifications and quality assurance provisions, were prepared. Negotiations of these documents with manufacturers were successfully completed and fully controlled high reliability parts were received at GE-SD starting in Spring 1962.

The selection of vendors who were considered capable of meeting the requirements of the procurement documents was performed by a team of purchasing, engineering, reliability, quality control and manufacturing personnel. Those vendors capable of meeting the requirements were designated as approved sources.

Since the problems of acceleration of degradation mechanisms and the determination of abnormalities in part performance related to each type of part are inherently different, each part type is considered separately. The investigation of screening techniques to eliminate weak parts from the production lots was conducted in close cooperation with the various part manufacturers. A series of control documents called Quality Assurance Provisions (QAP's) defines the screening tests applied to particular vendors. The general and detail specifications do in fact require certain screening tests for a part type, but the QAP is predominately dependent upon the manufacturing process of the particular vendor supplying the part. Thus, it has occurred that two manufacturers supplying parts to the same specification, were required to perform different screening tests, specified and monitored by GE-SD.

## 4.2 R-PART SPECIFICATIONS

Generally, the prescribed format for Military Procurement Specifications was followed in specifying the requirements for the R-Series high reliability parts. Two types of documents were prepared for each part. The first, a general specification, contains the similar requirements for part types such as metal film resistors, semiconductors, ceramic capacitors, etc., the second, a detailed specification, contains

the specific requirements, such as parametric values, acceptance tests, etc. of like part types. 156 detail specifications were prepared and approved for use.

The R-part Specifications provide for control of the parts beyond the MIL-SPEC quality assurances which are normally available to the user. Whereas, the MIL-SPECS provide for sampling acceptance inspection at both the user and the manufacturer, the high reliability R-part Specifications provide for the following additions:

a. Process control of selected lots of materials used in the manufacture of the high reliability part in all but proprietary processes. The lots are coded to provide for lot control.

b. 100 percent acceptance tests for defined parameters are performed at the vendor's plant plus lot sample environmental acceptance tests to tightened AQL's plus identification of lot, part and data by individual part and lot serialization numbers.

c. 100 percent receiving inspection and screening tests at GE-SD.

### 4.3 QUALITY ASSURANCE PROVISIONS

Generally, there are two Quality Assurance Provisions documents governing the quality control activity for each high reliability part type. The first is a general QAP and the second is a detail QAP. The general QAP specifies those controls which are common to all vendors such as data and information requirements, lot control, surveillance inspection, test equipment control, etc. The detail QAP specifies the acceptance tests, burn-in and screening tests, lot definition, etc. which are peculiar to each high reliability part. In the case where more than one vendor is an approved source for the part, a separate, detail QAP document exists for each vendor. This is necessary because the QAP contains process control requirements which are different depending upon the vendor's manufacturing process.

All R-series parts have a lot number and a serial number placed on them by the vendor at a point specified in the Quality Assurance Provision. The serialization number consists of two alphabetical digits for lot number combined with four numerical digits for serial number within the lot (i.e. AB-1234). A major problem in this area has been the definition of what constitutes a lot of parts and at what point in the manufacturing cycle a lot is formed. The QAP defines this point for each part type and vendor.

The necessity for providing automated data processing techniques and machinery for the part acceptance becomes obvious when the data point requirements are considered. Estimates of 400,000 parts for the prime hardware satellites were used in determining machine loading. The original assumption of over 12 million measurements which

require manipulation, based on an average of four parameter measurements per part and readings taken eight times during the acceptance test cycle, was found to be accurate as the program developed. The data processing equipment which is provided in the Parts Test Laboratory was adequate for the program. Automatic test stations were established which provide both absolute and drift parameter measurements during screening tests which are printed out on data processing cards. Various programs are provided for each part type and value so that the following manipulations of data may be performed by the computer:

a. Absolute parameter value tolerance comparison

b. Drift comparisons between data points

c. Lot mean and standard deviation for parameter measurements at each data point.

The reduced data thus derived, aside from providing the accept-reject decision serve as the basis for lot control of the parts, vendor data correlation, and studies of parameter stability.

The parts were received at the Parts Test Laboratory from the vendor in GE-approved shipping containers. After a paper work routine of logging in the parts, checking vendor supplied data, verifying serial numbers, etc. the parts were visually examined and placed on handling boards. The design of the boards and test equipment is such that the part will remain on the same board throughout the screening test cycle. The boards are provided with spring-loaded mounting posts, thus making them re-usable.

## 4.4 DISCUSSION OF SCREENING TESTS

### 4.4.1 General

With the requirement for long-life non-maintainable space vehicles of extremely high reliability, it becomes an economic necessity to provide assurance that each part of the flyable system will perform its mission for a minimum time period. In many cases limited usage of such parts does not justify the establishment of separate high reliability manufacturing lines for each part type. Instead, the practical approach has been 1) to obtain the maximum material and process controls at the vendors which can be economically justified, and 2) to perform a series of screening and acceptance tests on a 100 percent basis at the user's facility. Adequate precision measurements with proper analysis and control will then enable the user to separate parts which may not have the required design life potential from those which do.

4.4.2 Specification Controls

The present trend to the establishment of high reliability parts specifications has led to the general acceptance by the part manufacturers of quality controls of materials and processes which are superior to those which existed several years ago. Of course, the fundamental justification of sound quality control programs has also become apparent in higher product yields and more economical production. However, there is a limit to which a manufacturer can apply these advanced control methods and still maintain his competitive position in the mass market. Using existing controls as a basis for consideration, there rapidly approaches an economic limit to the establishment of additional tighter controls for high reliability parts. Negotiations of proposed high reliability specifications with manufacturers have shown this to be true. It is suggested here that individual program requirements will, with schedule and economic limitation, best be served by specifications which require controls which part manufacturers consider as adequate for long-life assurance. The established quality controls must be based upon a sound statistical foundation and enforced for each process and material used in the manufacturing cycle.

After the establishment of a basic series of high reliability parts specifications a concerted effort must be made to develop and use screening tests at the user's facility which are designed for individual program requirements.

4.4.3 Screening Tests

When selecting parts for use in long-life non-maintainable applications, it is essential that none of the parts have extraneous degradation or failure mechanisms. This means that all parts with other than the expected failure or degradation mechanisms, in addition to all defective parts, must be removed from lots destined for use. Screening tests are designed to accelerate or illuminate these foreign mechanisms by exercising the part through periods of time and environments.

Screening test failures, which are the result of isolated material and process anomalies, commonly constitute the "early failures", and are represented by the so-called "infant mortality" portion of the life curve shown below.

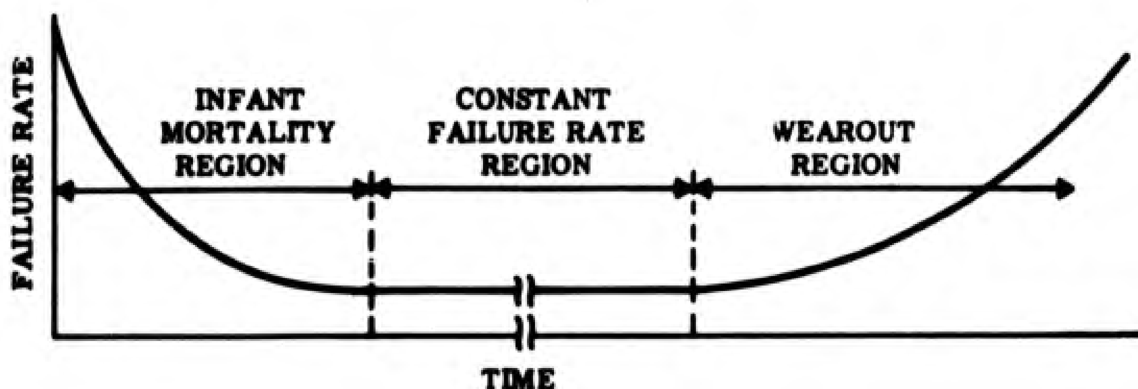

Electronic parts which follow this form of failure distribution are economically unacceptable for use in long-life space applications. A desirable and necessary distribution is shown below:

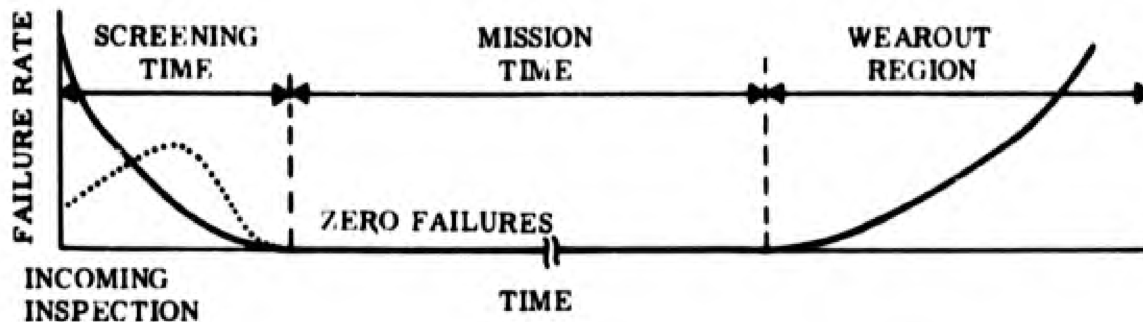


This life curve shows a long, failure-free period following screening tests. The separation of the failure regions into infant mortality and wearout is arbitrary. With the exception of failures due to extraneous causes such as extreme environments, equipment malfunction and the like, all normally expected failures would be due to wear out. These failures usually appear as the exceedance of a degradation limit. If a part sustains the stress initially, it will sustain it indefinitely unless some type of degradation mechanism is present.

Wearout is not to be confused with degradation; all parts degrade with time. Therefore, degradation is progressing during the entire lifetime of the part. Wearout occurs when the accumulated degradation exceeds some acceptable degradation or end-of-life limit which is often set at an arbitrary value for design usage limits. Actually the wearout distribution is more accurately described as illustrated below. This may be described by a Weibull distribution with a shape parameter $\beta < 1$.

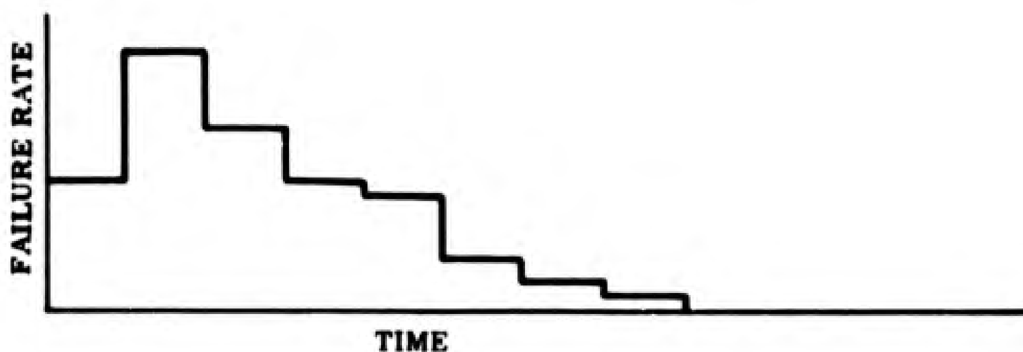


Of course, failure distributions for a particular part type can be determined only on a statistical sample basis. The RADC test program is designed to provide this information. In cases of extremely long life, test techniques designed to accelerate the degradation mechanisms are performed to provide life capability decisions in relatively short times.

#### 4.4.4 Parameter Drift Criteria

Screening tests are used in this program not only to eliminate the defective parts but also to detect parts which appear good against normal criteria, but which may fail to meet the life requirements, particularly as a result of parameter drift. These tests, performed on a 100-percent basis, include measurements of the standard parameters and of parameter drift rates during operational tests, (sometimes called "burn-in" tests), made in accordance with the R-Part high-reliability procurement specifications and of additional parameters or characteristics which may or may not be of direct operational significance.

The latter tests may indicate localized stress concentrations due to manufacturing imperfections. By correlation they are expected to make possible the identification and elimination from the population of those individual parts which have potentially short life expectancies.

#### 4.4.5 Screening Criteria

The inspection and screening tests that were applied to the R-series parts were developed by GE-SD, using the Military Specification criteria as a base, and with inputs from the part manufacturers. They specify close tolerances and extended operational tests of incoming parts in order to assure long-life reliability. A very important difference in emphasis exists between the screening required by GE-SD and that specified in MIL specifications. The Mil Spec is concerned with AQL's based on testing of samples, and hence a prediction of less than a given number of failures, whereas for space use every part must be reliable, and the goal is no failures. This demands 100 percent inspection and test of parts. Consequently, the spacecraft manufacturer is faced with the added problem of eliminating those parts which pass the manufacturers' tests, but which may be inferior in more subtle respects.

The criteria for acceptance of parts are based upon:

1. The homogeneity of product, before and after screening tests
2. The rate of change of parameters, during screening tests
3. Over stress tests consistent with the intended use of the part.

Homogeneity of the parts may be determined from initial parameter measurements and from measurements made before and after dynamic-performance or environmental tests. Statistical tests for significance may be made on the distribution, and dissimilar parts may then be removed from the population.

For an electronic part, homogeneity must be interpreted with respect to the specific part and its parameters. There is a difference between parameter measurements

which reflect relatively stable mechanical/electrical parameters and those parameter measurements which are expected to change or degrade in time. For example, the capacitance of a glass capacitor and the initial resistance of a metal resistor are both results of the accuracy controls imposed on the respective manufacturing processes, and variations from nominal are thus not normally expected to have any effect on reliability. On the other hand, dissipation factor of a capacitor and current noise of a resistor are affected by actual errors in manufacture which cause inherent defects in the part and thus substandard values can definitely be related to reliability.

Rate of changed parameters is also an important element in screening. Changes resulting from bake tests, overload tests, "burn-in" tests, and others which are benign to the best long-life parts but harsh toward the abnormal parts, are measured. Illustrated below are hypothetical parameter measurements as a function of time:

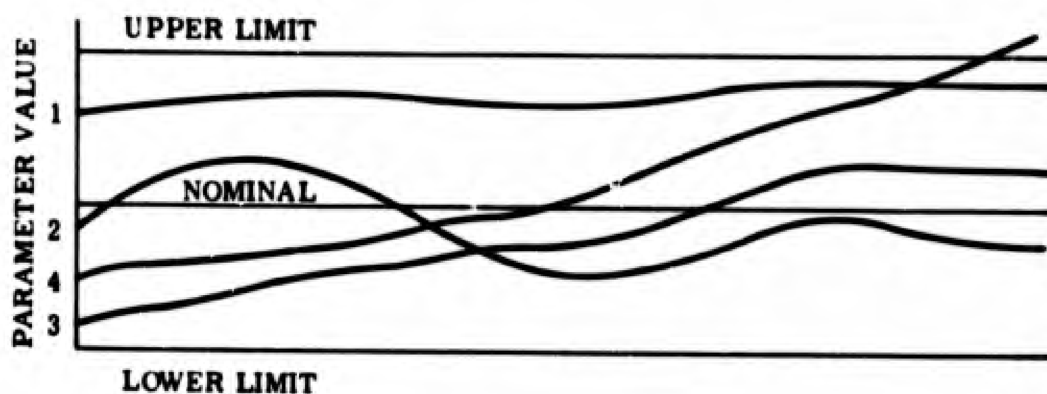


Parts 1 and 3 are behaving as expected (Part 3, of course, after a stabilization period); Parts 2 and 4 are degrading at abnormal rates. Part 4 has already exceeded the upper limit; and Part 2 is not acting in the acceptable manner and may fail early.

Homogeneity, in the form of similar changes of parameter values, is thus required in addition to similarity of the parameter values themselves. Examples of screening tests for which conformance to maximum parameter change limits are specified are semiconductor bake tests and resistor overload tests.

Some types of parts show no measurable change in parameters over very long periods of operation. For instance, glass capacitors generally show no change in capacitance, insulation resistance of dissipation factor, but ultimately may fail catastrophically. This does not mean that the parts are not degrading in time. If it were possible to measure ion migration and progress of microstructural imperfections by a non-des destructive method, then the rate of degradation could be determined thus providing a more accurate prediction of life. The screening test that has proven most useful in eliminating weak parts for this type capacitor is a 50-hour proof test at 1500 volts (i.e., in the range of three or five times the rating).

#### 4.4.6 Linear Discriminants

In the preceding discussion it is assumed that defective parts may be identified by the results of parameter measurements, either initially or by the changes occurring during a relatively short operational test. It is also possible to combine the results of several parameter measurements and, hopefully, arrive at a better prediction.

A prediction method using linear discriminents is based on a weighted average of the significant parameters. Problems in the application of the method are: the determination of the parameters which are significant in predicting failure, the determination of the weight that should be assigned to each and the transformation required to make the data fit a normal distribution. Mr. M. F. Chamow presented a paper entitled "A Reliability Prediction for Semiconductor Devices" at the Third Annual Symposium on Physics of Failure in Electronic Parts in which he discussed the use of this technique applied to data taken from the Advent parts evaluation program.

# 5. SUMMARY AND CONCLUSIONS

Upon review of the test data and failure mechanism studies performed during the Advent Parts Evaluation Program, several improvements were found to be advisable in the design of the tests for this program. The changes were incorporated in the test specifications and all accelerated step-stress and constant-stress tests were started as scheduled. The analysis procedure to be used has been specified for two general conditions of failure; i.e. drift of measurable part parameters and catastrophic failures. The detailed analysis techniques for the resistor and capacitors part types have also been specified. A technique for analysis of semiconductor test results based upon exceedance of a defined failure criteria has been established but work is continuing on developing a method which will be based upon the analysis of the rate of semiconductor parameter degradation. Investigations are continuing in an effort to establish the techniques for determining the correlation factors between the accelerated tests and normal usage life tests.

The physics of failure studies and tests have led to the formulation of physical models for degradation of metal film resistors, ion migration in glass dielectric capacitors and surface contamination of planar transistors. The validity of these models will be assessed during the next reporting period.

No technical conclusion may yet be drawn from the data in this the first four-month reporting period.

BLANK PAGE

# 6. WORK PLANNED FOR THE NEXT PERIOD

## 6.1 RESISTORS

It is planned to continue the constant stress tests and Phases II and III step stress tests of the resistors on test. Analysis of the step stress and constant stress data as they are obtained will be made to confirm the relations tentatively established. Efforts will be made to determine the probabilistic characteristics of the populations of resistors of different types so that extremes as well as means can be predicted. The effectivity of the screening tests on the basis of the life test results will be evaluated. All data will be available in format for computer manipulations.

Measurements of resistance profile along the film will be made to characterize by geometry by microstructure the areas in the films which produce maximum drift.

## 6.2 CAPACITORS

During the next reporting period it is expected that the expression for the leakage current from 100° to 225°C and its relationship to the ionic transport equilibrium model will be established. Calculations associated with the model will be extended to determine whether electronic breakdown is predicted by this model at ionic equilibrium. The charge-discharge technique will be used to provide a better estimate of the d-c dielectric constant and the dielectric relaxation time. Additional study will be devoted to interpreting possible effects of transient phenomena on the equilibrium model, including the consistently noted rise-time effect.

A switching circuit employing a thyratron tube will be constructed to minimize switching transients found in the test circuit for times less than one millisecond; impulse voltages of various rise times and magnitudes will then be applied to devices.

## 6.3 SEMICONDUCTORS

It is planned to devote a considerable amount of effort to establish an experimental basis for the postulated degradation model and to establish whether the detected contaminant can cause the observed phenomena in the various types of transistors. In addition, the test data indicate that certain transistors are drifting and failing primarily by degradation of the ohmic contacts; therefore an investigation of these will be initiated. The step stress and constant stress tests will be continued at the present rate.

Rate expressions will be established for the expected degradation mechanisms and studies made of the test data to provide a deterministic approach for predicting semiconductor life-times.

### 6.3.1 Surface Effects Investigation

To investigate the surface phenomena, as related to apparent surface effect behavior in the semiconductors and the detection of the phosphide and phosphorous compounds, and to develop the functional form of the drift in terms of the independent variables, it is planned to expose new opened devices to various pressures (or partial pressures) of these contaminants, with various levels of device temperature and operating conditions. At least $I_{CBO}$ and $h_{FE}$ will be measured.

The facility, as planned, can be set up from existing equipment and will meet certain requirements. It will be electromagnetically shielded, bakeable, and simultaneously evacuable to $10^{-9}$ torr. Controlled amounts of contaminating material can be introduced and the mounted device can be heated, biased, and monitored for electrical parameter charges. The contaminant pressure will be measurable and the system can be monitored by a mass spectrometer.

### 6.3.2 Ohmic Contact Investigation

The second principal mode of degradation observed on the transistors is ohmic contact degradation, including loss of mechanical continuity increase in series resistance, and junction penetration. This will require a separate metallurgical investigation to establish the functional dependence of the electrical and mechanical characteristics. The metallurgical system is established by depositing on, and alloying a thin film of aluminum to, the silican substrate. A gold wire is then thermo-compression bonded to the aluminum-silicon system. Though both aged and unaged (new) devices are available for comparison, it is believed that determination of the correlation with life expectancy of the part will require the preparation of special specimens.

Though a study using new devices will be considered, if simulated devices are chosen, these will be prepared by simulating the manufacturing process. Geometry will be modified to facilitate the investigation procedure. A time-temperature aging study in a nitrogen ambient will then be performed on these samples. This study will include monitoring electrical characteristics and performing metallurgical studies, the latter including optical and electron microscopy and electron diffraction. It is anticipated that electron microscopy will be required to follow the degradation precess and electron diffraction may be necessary in some instances for identification of phases or intermetallics. Additional specimens will be prepared and aged for mechanical strength tests.

## APPENDIX I. DERIVATION OF THE $\theta$ PARAMETER

Presuming that the reactions which result in resistance change are zero or first-order, and that some function of resistivity is dependent on the progress of the reaction, a rate expression can be formulated as follows (This derivation assumes zero order which is generally conceded to be true for diffusion dependent reactions):

$$\text{rate} = \frac{d\, f(R)}{dt} = K_r \tag{1}$$

where:

$f(R)$ = function of resistance

$K_r$ = reaction rate constant

$t$ = time

The reaction rate constant $K_r$, according to the Theory of Absolute Reaction Rates, is dependent on temperature as follows:

$$K_r = \frac{KT}{h} e^{\Delta S/Rg} e^{-Q/RgT} \tag{2}$$

where:

$K$ = Boltzmann's Constant

$T$ = Absolute Temperature

$h$ = Planck's Constant

$S$ = Entropy of Activation

$Q$ = Activation Energy

$R_g$ = Gas Constant

For a resistance value read at time t, an approximate relationship can be written:

$$\frac{R - R_o}{R_o} = \frac{KT}{h} e^{\Delta S/Rg} e^{-Q/R_g T} t \tag{3}$$

Taking logarithms,

$$T \log \frac{R - R_o}{R_o} + \frac{Q}{2.3} R_g = T\ (\text{Const} + \log t) \qquad (4)$$

$$\text{where Const} = \log \frac{KT}{h} e^{\Delta S/R_g}$$

This derivation shows the relationship between absolute temperature and the logarithm of time. Plotting the logarithm of some function of resistance versus a parameter of the form:

$$\theta = T\ (\text{Const} + \log t)$$

for a variety of test exposures should produce a straight line for a single reaction which results in a change in resistance. Previously reported results of tests conducted on metal film resistors indicate the utility of this approach.

It is to be observed, of course, that both $\theta$ which lumps the entire lefthand side of Equation (4) and the constant (Const.) are functions of temperature. This is certain to introduce error into the expression. The amount of this error is not known. However, this error is apparently sufficiently small, as indicated by the degree of fit to the test data taken at various temperatures spanning the range of device application, that the value of having a time-temperature trade-off expression for predicting life is not seriously affected.

## APPENDIX II. DERIVATION OF MODEL FOR SODIUM IONS AT EQUILIBRIUM WITH FIELD IN GLASS CAPACITORS

The working model of the system is as follows. A dielectric of thickness L and dielectric constant D contains mobile positive ions, whose concentration $\rho^+$ is a function of x in an applied field, and immobile negative ions whose concentration $\rho^-$ is independent of x.

The electrochemical potential of positive ions is given by

$$\mu = \mu^0 + RT \ln \rho^+ + ze\psi \tag{1}$$

where $\mu^0$ is a function of temperature and the nature of the dielectric but independent of concentration and $\psi$ is the electrostatic potential. ze is the charge on the ion. At equilibrium $\mu$ must be independent of x and hence $\mu - \mu_0$ must be independent of x. Therefore at equilibrium

$$\frac{\partial(\mu - \mu_0)}{\partial x} = \frac{\partial^2(\mu - \mu_0)}{\partial x^2} = 0 \tag{2}$$

Poissons equation holds in the dielectric

$$\frac{\partial^2 \psi}{\partial x^2} = -\frac{4\pi}{D}(\rho^+ - \rho^-) \tag{3}$$

If equations 1, 2 and 3 are combined, a second order non-linear differential equation is obtained whose solution, with the appropriate boundary conditions determines $\rho^+$. A simple and excellent approximation, however, obviates the necessity of solving a non-linear differential equation.

We define the quantity g (x) by the relation

$$\rho^+ = \rho^- + g \tag{4}$$

g represents the net charge and for reasonable ion concentrations and applied fields and it is true that

$$g << \rho^+$$
$$g << \rho^- \tag{5}$$

Assume Equation (5) to be valid in the following. Equation (1) may be rewritten as

$$\mu - \mu^{o} = RT \ln (1 + g/\rho^{-}) + RT \ln \rho^{-} + ze\psi \tag{6}$$

and if the first logarithm on the r.h.s of Equation (6) is expanded and only the first term is kept, obtain

$$\mu - \mu_{o} = RT g/\rho^{-} + RT \ln \rho^{-} + ze\psi \tag{7}$$

If the second derivative of Equation (7) is equated to zero and Equations (3) and (4) are utilized,

$$\frac{RT}{\rho^{-}} \frac{\partial^{2} g}{\partial x^{2}} - ze\frac{4\pi}{D} g = 0 \tag{8}$$

The general solution of (8) is

$$g = A \ell^{\sqrt{c}\, x} + B \ell^{-\sqrt{c}\, x} \tag{9}$$

with

$$C = \frac{ze 4\pi \rho^{-}}{DRT} \tag{10}$$

A and B are integration constants. One of these constants may be eliminated by invoking the principle of electroneutrality of the entire dielectric. Using this in equation (4) leads to the expression

$$\int_{-L/2}^{L/2} g \, dx = 0 \tag{11}$$

This in turn shows that

$$A = - B \tag{12}$$

hence

$$g = A(\ell^{\sqrt{c}\, x} - \ell^{-\sqrt{c}\, x}) \tag{13}$$

If Equations 3 and 13 are combined there results

$$\frac{\partial^2 \psi}{\partial x^2} = - \frac{4\pi}{D} A \left( \ell^{\sqrt{c}\, x} - \ell^{-\sqrt{c}\, x} \right) \tag{14}$$

The general solution of Equation (14) is

$$\psi = \alpha x + B - \frac{1}{C} \frac{4\pi A}{D} \left( \ell^{\sqrt{c}\, x} - \ell^{-\sqrt{c}\, x} \right) \tag{15}$$

The boundary conditions are as follows:

$$\psi = - V/2 \qquad x = - 1/2 \tag{16}$$

$$\psi = V/2 \qquad x = 1/2 \tag{17}$$

$$+g = 0 \quad \text{when} \quad V = 0 \tag{18}$$

Comparison of Equations (13) and (18) lead to the results

$$A = 0 \text{ when } V = 0$$

$$\therefore \alpha = 0 \tag{19}$$

The expression for the potential is

$$\psi = V/2 \, \frac{\left( \ell^{\sqrt{c}\, x} - \ell^{-\sqrt{c}\, x} \right)}{\left( \ell^{\sqrt{c}\, L/2} - \ell^{-\sqrt{c}\, L/2} \right)} \tag{20}$$

and the expression for g is

$$g = \frac{V C D \left( \ell^{\sqrt{c}\, x} - \ell^{-\sqrt{c}\, x} \right)}{8\pi \left( \ell^{-\sqrt{c} L/2} - \ell^{\sqrt{c} L/2} \right)} \tag{21}$$

g is a monotonic function of x. It is also to be noted that this expression does not reduce to a Boltzman relation when $\rho^-$ and C approach zero. Under these circumstances Equation (5) is not valid.

Equations (20) and (21) may be rewritten as

$$x = \frac{V}{2} \frac{\sinh \sqrt{c}\, x}{\sinh \sqrt{c}\, L/2} \tag{22}$$

$$g = -\frac{V C D}{8 \pi} \frac{\sinh \sqrt{c}\, x}{\sinh \sqrt{c}\, L/2} \tag{23}$$

## APPENDIX III. ADDITIONAL DEVELOPMENT OF THE EXPRESSION FOR CALCULATING ELECTROSTATIC POTENTIAL AND ELECTRIC FIELD AT ION TRANSPORT EQUILIBRIUM

The electrostatic potential $\psi(x) = \psi(g(x))$, caused by the ion distribution at equilibrium only, is

$$\psi(g(x), t_e) = + \frac{V}{2} \frac{\sin h\,(\sqrt{c}\,x)}{\sin h\,(\sqrt{c}\,\frac{L}{2})}$$

where $\psi(g(x), t_e)$ is used to distinguish that component of $\psi(x)$ associated with the modified ion distribution.

The total electrostatic potential is the algebraic sum of the initial dc field and the component just derived. For this approximation, it will be assumed that the dielectric is homogeneous and isotropic. The initial field seen by the dielectric is then

$$E = \frac{E_o}{\epsilon_r} \text{ in cgs units} \qquad (1)$$

where

$E_o$ is the applied field

and

$\epsilon_r$ is the relative dielectric constant.

From

$$E_o = -\nabla V_o = -\frac{Vo}{L}$$

by the assumptions of this instance, the applied potential seen within the dielectric is

$$V = -EL = -\frac{E_o L}{\epsilon_r} = \frac{Vo}{\epsilon_r} \qquad (2)$$

where Vo is the applied potential.

Using the geometric conditions stated in the derivation of $\psi$ (g(x)),

$$-\frac{L}{2} \leq x \leq L/2$$

and correspondingly

$$-\frac{V}{2} \leq \psi(x, t_o) \leq \frac{V}{2}$$

where

$$\psi(x, t) = \psi(x, t_o)$$

implies that $t_o$ exists as a time at which dielectric polarization is essentially complete, except for that associated with ion migration which is not yet significant. Then

$$\psi(x, t_o) = \frac{V_o}{2\epsilon_r} \frac{x}{L/2} = \frac{V_o x}{\epsilon_r L} \tag{3}$$

The fact that the absorption current at 100°C requires nearly a week to decay to the leakage current value suggests an as yet undetermined error in implying that $t_o$ exists as defined.

At the time of ion equilibrium, ($t_e$),

$$\psi(x, t_e) = \psi(x, t_o) + \psi(g(x), t_e)$$

or

$$\psi(x, t_e) = \frac{V_o}{\epsilon_r} \frac{x}{L} + \frac{V_o}{2\epsilon_r} \frac{\sin h\sqrt{c}\, x}{\sin h\sqrt{c}\, L/2} \tag{4}$$

This expression predicts that after equilibrium occurs, $\psi(x, t) = 0$ at $x = -L/2, 0, L/2$ regardless of the temperature or the applied voltage within the applicable range of voltage and temperature.

For this one dimensional problem

$$E(x, t_e) = \frac{\partial \psi}{\partial x}(x, t_e) = -\frac{V_o}{\epsilon_r L} - \frac{V_o}{2\epsilon_r} \frac{\sqrt{c}\cosh\sqrt{c}\, x}{\sin h\sqrt{c}\, L/2} \tag{5}$$

This expression predicts that E will be largest at $X = \left| \frac{L}{2} \right|$ and at lower temperatures since $c \; \alpha \; \frac{1}{T}$

Since one of the goals of this model is to establish the maximum and minimum predicted electrostatic potentials, the values of x at which $\nabla_x \psi = 0$ is needed. By the symmetry involved, only $|x|$ is needed.

$$\nabla_x \psi (x, t_e) = 0 = + \frac{V_o}{\epsilon_r L} + \frac{V_o \sqrt{C}}{2 \epsilon_r} \frac{\cosh \sqrt{C}\, x}{\sinh \sqrt{C}\, L/2} \tag{6}$$

or

$$\frac{1}{L} = \frac{\sqrt{c}}{2} \frac{\cosh \sqrt{C}\, x}{\sinh \sqrt{C}\, L/2}$$

transposing,

$$- \frac{2}{C} \frac{1}{L} \sinh \sqrt{C}\, L/2 = \cosh \sqrt{c}\, x$$

and

$$X = \frac{1}{\sqrt{C}} \cosh^{-1} \left[ \frac{-2}{\sqrt{C}} \frac{1}{L} \sinh \sqrt{C}\, L/2 \right] \tag{7}$$

BLANK PAGE

# APPENDIX IV. DEVELOPMENT OF NUMERICAL VALUES TO BE USED IN CALCULATING ELECTROSTATIC POTENTIAL AND ELECTRIC FIELD

To perform calculations for either E (x) or $\psi$ (x), the constant C must be evaluated. Principally, an estimate of $\rho^-$ must be made and values for the d-c dielectric constant obtained.

Assuming that sodium is the predominant mobile ion and that the value of $\rho^-$ is equal to the number of sodium ions,* similarly called $\rho^+$, $\rho^+$ (or $\rho^-$) is estimated from the measured percent by weight content in the glass. This was estimated by -

$$W_{Soda(g)} \times \rho_g = \rho_{Soda(g)}$$

$$\frac{M_{Na}}{M_{Soda}} \times \rho_{Soda(g)} = \rho_{Na(g)}$$

$$\frac{\rho_{Na(g)}}{\rho_{Na}} \times \frac{N}{V_{mole(Na)}} = \rho^-$$

where the subscripts are defined as -

soda ⟶ $Na_2O$

Na ⟶ sodium

(g) ⟶ in the glass

and the definitions and values of the quantities used and obtained are:

$W_{Soda(g)}$ = weight percent of soda in the glass = 3.82 percent for $W_{Soda(g)}$

$\rho_g$ = density of glass = 3.824 gms/cc

$\rho_{Soda(g)}$ = density of soda in the glass = .146 g/cc

*Note: $\overline{g(x)} = \frac{1}{L}\int_0^L g(x)\,dx = 0$ is obviously not incompatible with $g(x) \neq 0$

$M_{Na_2}$ = Atomic weight of $Na_2$ = 46

$M_{Soda}$ = Atomic weight of $Na_2O$ = 62

$\rho_{Na(g)}$ = density of sodium in the glass = .1082 gm/cc

N = Avogadro's number = $6.02 \times 10^{23}$/mole

$V_{mole(Na)}$ = Molar volume of Na = 23.75 cc/mole

$\rho^-$ = $2 \times 10^{21}$/cc

The values of $D = E_0E$ to be used have not been established. D is the dc dielectric constant which is usually somewhat greater than that at a megacycle. Only values at a megacycle are currently available on this glass. Since the 8871 glass has been shown to have an extended absorption current time, the d-c dielectric constant at equilibrium may be significantly larger than that at a megacycle. Since the values of $\psi$ and E are inversely dependent on $D = D(t_e, T)$, the use of the megacycle value contributes to an over-estimation of their values at equilibrium.

Z will be assumed to have an effective value of one, i.e., the oxygen ions will in general lose only one of the $Na^+$ ions and thereby be singly ionized. It is doubtful that the quantity of double ionization will significantly affect the model.

The values of the constants to be used in evaluating $\psi$ and E are summarized as

$Z = 1$

$e = 4.8 \times 10^{-12}$ e s u

$\pi = 3.14$

$\rho^- = 2 \times 10^{+21}$ charge/cc

$R = 8.317 \times 10^7$ ergs/degC/mole

$\left|\frac{L}{2}\right| = 1.8 \times 10^{-3}$ cm (i.e., 0.7 mil)

T will be expressed in °K and since D is in c g s units

$$D = \epsilon_0\epsilon_r(T) = \epsilon_r(T)$$

At one megacycle, values of $\epsilon_r$ (T)* are -

25°C - 8.4

100°C - 8.5

200°C - 8.7

300°C - 9.0

375°C - 9.5

Note that $V_o$ (in c g s) = $V_o$ (in M K S) x $\frac{10^6}{c}$, where c is approximately 3 x $10^8$ meters/second.

---

*Barney, W.H., Dielectric Behavior of Glasses and Glass Ceramics, Fourth Electrical Insulation Conference, AIEE, T-137-38, pp. 83-84.

# APPENDIX V. THE ULTRAVIOLET ABSORPTION EDGE AND CALCULATION OF FORBIDDEN ENERGY GAP

Two specimens were measured. One was 19 mils thick and the other 2.8 mils. These were obtained from the vendor and are believed to represent two stages in rolling reduction of the glass strip. The maximum transmission of incident radiation was 88 percent and 85-1/2 percent for the 2.8 mil and 19 mil strips respectively. The absorption edge was selected as 1/e of these values, i.e. 32.23 and 31.45 percent transmission, corresponding to 2100 Å and 3250 Å.

To calculate $E_G$:

$$E_G = h\nu = h\frac{c}{\lambda}$$

$$= \frac{6.627 \times 10^{-27} \text{ erg cm} \times 2.998 \times 10^{10} \times \text{cm/sec}}{3.1 \times 10^{3} \text{ Å} \times \frac{\text{cm}}{10^{8}\text{ Å}} \times 1.602 \times 10^{-12} \text{ ergs}}$$

$$= \frac{19.868 \times 10^{-17} \text{ ev}}{1.602 \times 3.1 \times 10^{3} \times 10^{-20}}$$

$$= \frac{12.402 \times 10^{-3} \text{ ev}}{3.1 \times 10^{-3}}$$

$$= 4.001 \text{ ev.}$$

For the 19 mil material,

$$E = \frac{12.402 \times 10^{-3} \text{ ev}}{3.25 \times 10^{-3}}$$

$$\doteq 3.802 \text{ ev}$$

Select 3.9 ev. as a value to be used in the evaluation of the component of $\psi$ and $-\nabla\psi$ induced by the ions.

# APPENDIX VI. EQUIPMENT AND PROCEDURES USED IN MEASURING CAPACITOR ABSORPTION AND LEAKAGE CURRENT

## 1. LONG TIME CURRENT MEASUREMENT EQUIPMENT AND PROCEDURE R2045P151 (150 PF)

Current measurements were made by placing the capacitor in an electrostatically shielded temperature chamber controlled to ± 0.1°F. The capacitor was supported rigidly within the chamber and shielded leads were brought out through tight-fitting access holes in the chamber door.

Direct voltage for the measurements was obtained from a Keithley Model 240 Regulated D-C Power Supply having output voltages adjustable from 0 to 1000 volts and calibrated so that the output voltage settings (by panel controls) were accurate to 0.1 percent. The regulation of this supply is such that, when the 150 pf capacitor load is applied, the voltage recovers to its nominal value in about 2 milliseconds as determined by cathode-ray oscilloscope.

The current through the capacitor was measured with a Keithley Model 410 Micromicroammeter having an accuracy within ±2 percent of full scale from $10^{-4}$ to $10^{-9}$ amperes and within 4 percent for currents from $10^{-10}$ to $10^{-13}$ amperes. Since this instrument has a constant input IR drop of 5 millivolts, which is negligible in comparison with the test voltages, the voltage applied to the capacitor has been assumed to be equal to the calibrated output voltage of the d-c power supply. The test circuit is shown schematically in Figure VI-1.

Prior to each test the capacitor within the chamber was short-circuited, the chamber temperature raised to 300°C and maintained at that temperature for about 16 hours to remove significant previous electrical history.

For each measurement the chamber temperature was lowered to the desired value, the capacitor short circuit removed and the part allowed to stabilize at the measurement temperature for 1 hour. The desired voltage value was pre-set on the power supply; when the voltage output switch was turned on, a timer started simultaneously. The Micromicroammeter scale selector was adjusted to the proper scale within 2 seconds and the first current reading taken at 5 seconds. (An initial high current scale setting on the Micromicroammeter substantially reduced the series resistance during capacitor charging.) No reading was taken in less than 5 seconds because the Micromicroammeter has a rise time on the low current scales such that accurate readings cannot be obtained in less than about 4 seconds. Subsequent current readings were taken at 5-second intervals for at least the first minute after voltage application and at longer intervals thereafter.

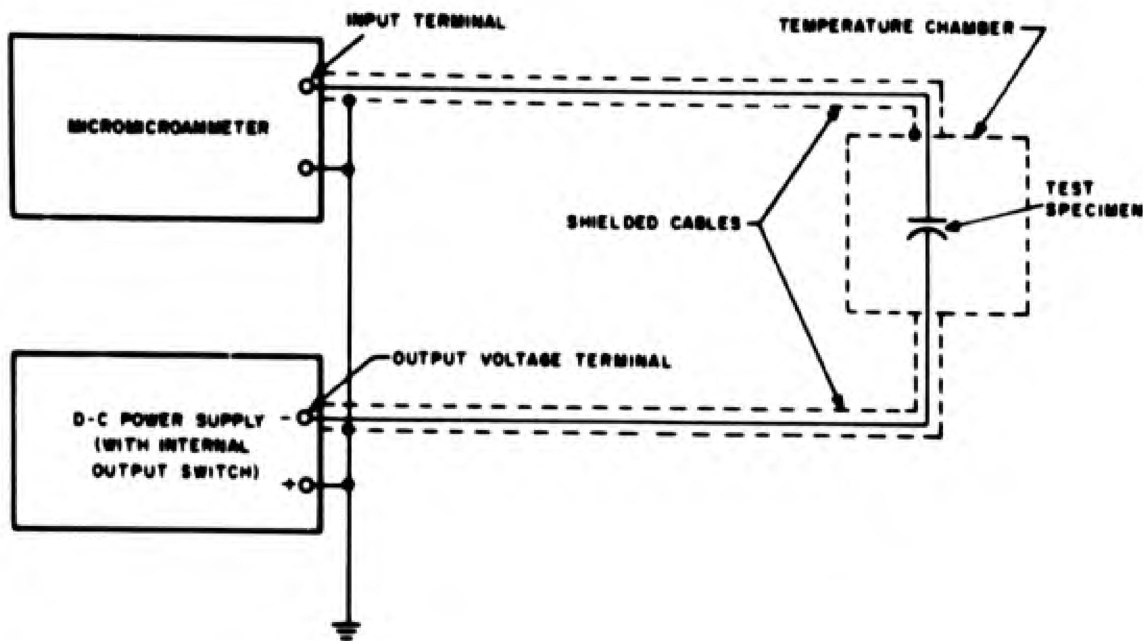


Figure VI-1. Schematic Circuit For Long Time Current Measurements in R2045P151 Capacitors

Since the power supply has an output impedance of 15 ohms, the 150 pf capacitor can be considered to be fully charged in 150 x $10^{-12}$/(farads) x 15 (ohms) x 10 or 2.25 x $10^{-8}$ seconds from voltage application. However, the power supply has a recovery time of 2 x $10^{-3}$ seconds; therefore, the capacitor can be considered to have been fully charged in 2 x $10^{-3}$ + 2 x $10^{-8}$ seconds or in 2 x $10^{-3}$ seconds. Hence all currents read for times of five seconds or greater are considered to be adsorption and leakage currents only.

Using this technique, current measurements were made at 20, 100 and 500 volts at temperatures of 100°, 150° and 225°C.

## 2. SHORT-TIME CURRENT MEASUREMENT EQUIPMENT AND PROCEDURE R2045P151 (150 PF)

The discussion of the long time current measurements which were made for times of 5 seconds to many thousands of seconds has indicated that the limitations of the voltage source and the charging time of the capacitor prevent accurate measurement of polarization and anomalous currents at times less than about 2 milliseconds. Experiments

were made to determine current values for the time interval between 2 milliseconds and 5 seconds. This necessitated the use of different current measuring equipment and techniques. The temperature chamber and its internal capacitor mounting as well as the voltage-history removal procedure were retained.

For the short-time measurements the circuit of Figure VI-2 was used.

The Keithley Model 210 D-C Power Supply is the source of power although it had been determined that its output was not stable before $2 \times 10^{-3}$ seconds after turn-on of the output voltage switch. This put a lower limit on the time at which current could be investigated, but experimentation with a battery voltage source and available switches for applying voltage to the capacitor showed that switching transients, the (minimized) circuit lead inductance, and the input characteristics of the amplifier prevented obtaining the desired voltage across the capacitor in less than $2 \times 10^{-3}$ seconds. Hence, the Keithley source was employed.

The resistor used is non-inductive. Its $1.88 \times 10^6$ ohm value ensures essentially complete charging of the capacitor in $2.5 \times 10^{-3}$ seconds, which was chosen as the minimum time at which polarization current could be determined.

The Keithley Model 603 Electrometer Amplifier is capable of amplifying voltages from d-c to 500 kc. Tests of its output showed its rise time was not greater than $1 \times 10^{-7}$ seconds which is ample for following the adsorption current decay in the capacitor. This instrument has a gain adjustable from 10 to 4,000. Its sensitivity and output characteristics prevented measurement on the oscilloscope of currents at times greater than $2 \times 10^{-2}$ seconds for the 100C measurements made to date.

The Tektronix Type 545A Cathode Ray Oscilloscope is fitted with a Tektronix Type K Preamplifier. The preamplifier has a rise time of $6 \times 10^{-9}$ seconds and the basic scope has a rise time of $12 \times 10^{-9}$ seconds. In combination with the Keithley amplifier, the scope is well able to follow the change of current through the capacitor.

In making the current measurements from $2.5 \times 10^{-3}$ to $2 \times 10^{-2}$ seconds, the fully discharged capacitor was brought to the test temperature in the temperature chamber and allowed to stabilize for 30 minutes prior to test. An appropriate amplifier gain was selected together with the proper CRO sweep rate and vertical deflection sensitivity. The output switch of the d-c power supply was closed, charging the capacitor and triggering the CRO. The CRO vertical deflection was read at various horizontal positions of the sweep.

The time was calculated from the sweep rate in milliseconds/centimeters and the horizontal deflection in centimeters. The current at this time was calculated from the IR drop across the resistor and the resistor value ($1.88 \times 10^6$ ohms) by Ohms Law, $I = \frac{E}{R}$ where:

$$E = \frac{\text{CRO vertical sensitivity (volts/cm)} \times \text{vertical deflection (cm)}}{\text{amplifier gain}}$$

The overall accuracy of current measurement is estimated to be ±10 percent.

Thus far, this equipment has been used to measure the current in a capacitor charged to 500 volts at 100°C.

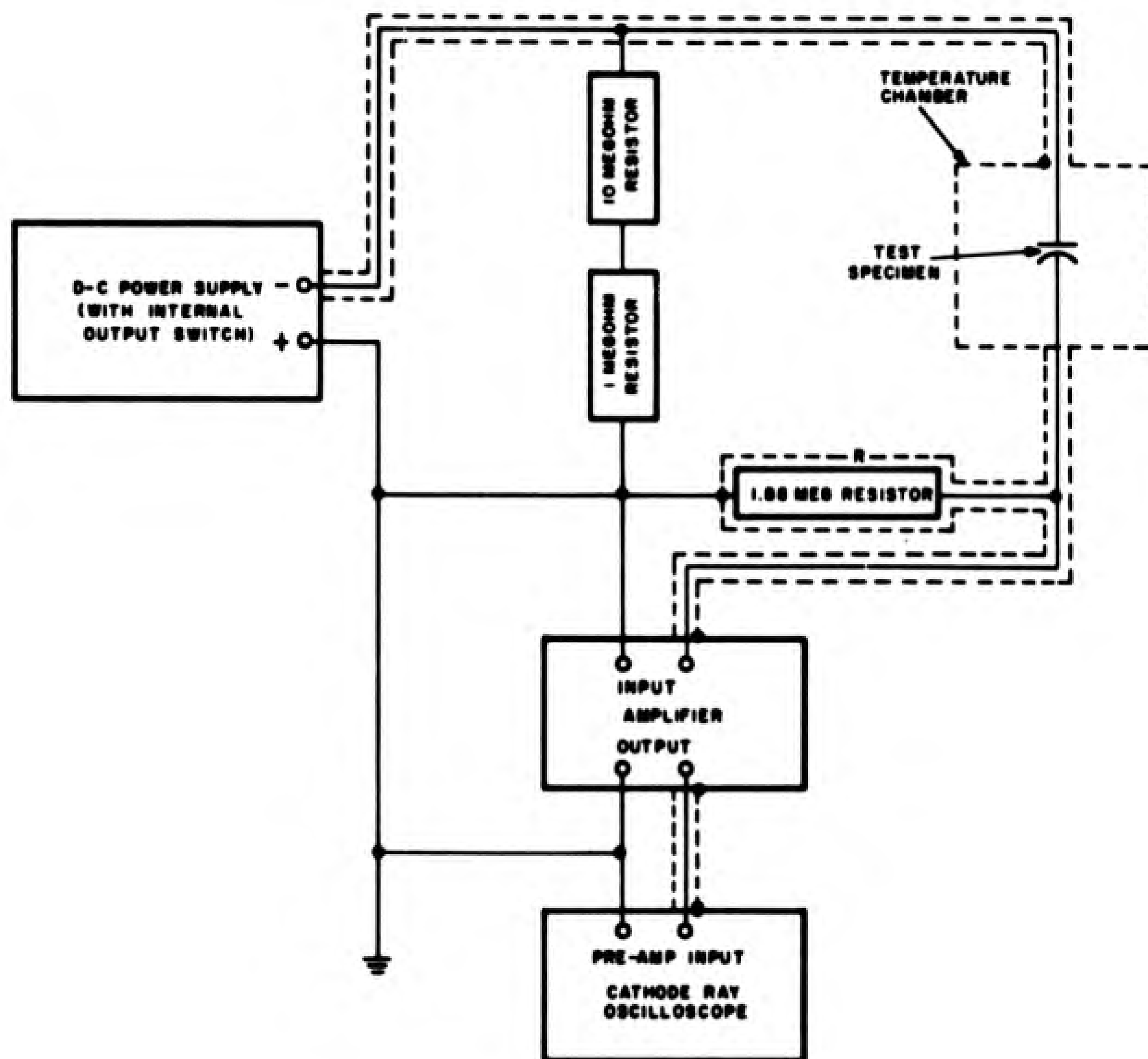


Figure VI-2. Schematic Circuit For Short Time Current Measurement in R2045P151 Capacitor

## APPENDIX VII. DIODE HEAT TRANSFER STUDY

Measurements were made of the relative proportions of the heat dissipated from the leads and from the body of a glass body diode mounted in a copper block. Values between 50 and 94 percent were found for various test configurations. The principal variable was the contact between the glass housing of the diode and the copper block. The copper block was used as a calorimeter. The diameter of the hole in the block and the heat transfer medium between the diode and block were varied. The leads were connected to ceramic standoffs. For one test copper clips were also connected to the leads near the glass body.

The physical and controlled variable data of each test are given in Table VII-1. In conducting each test, a fixed power was dissipated in the test diode for a period of five or six minutes while the temperature rise of the copper block was monitored with an imbedded thermocouple. A total temperature rise of 1 to 2°C occurred during this period. At the end of the powered period, current was turned off, and the decrease in temperature of the copper block over a five-minute period was measured with the thermocouple. From the measured values, the amount of heat transferred to the copper block was calculated.

TABLE VII-1. MEASURED QUANTITIES FOR EACH TEST

| TEST | 1 | 2 | 3 | 4 | 5 | 6 |
|---|---|---|---|---|---|---|
| Mass of Copper (grams) | 56.29 | 56.29 | 52.3 | 52.3 | 52.3 | 52.3 |
| Heat capacity of Copper (cal/gram) | 0.092 | 0.092 | 0.092 | 0.092 | 0.092 | 0.092 |
| Power input to diode (watts) | 0.154 | 0.154 | 0.154 | 0.154 | 0.156 | 0.185 |
| Diode body diameter (inches) | 0.098 | 0.098 | 0.098 | 0.098 | 0.098 | 0.098 |
| Diameter of hole in copper (inches) | 0.100 | 0.100 | 0.140 | 0.140 | 0.140 | 0.140 |
| Contact between diode and copper block | tight fit | tight fit | line contact | none | Silicone grease | Silicone grease aged 30 days at 200°C |
| Lead contact | to stand-off | to stand-off + copper clips | to stand-off | to stand-off | to stand-off | to standoff |

Table VII-2 gives the thermocouple readings in microvolts during the powered and cooling portion of each test. Calculated results are given in Table VII-3 and a sample calculation is included.

TABLE VII-2. THERMOCOUPLE MEASUREMENTS IN MICROVOLTS (40 MICROVOLTS = 1°C)

| TEST 1 | | TEST 2 | | TEST 3 | | TEST 4 | | TEST 5 | | TEST 6 | |
|---|---|---|---|---|---|---|---|---|---|---|---|
| TIME | $\mu$V | TIME | $\mu$V | TIME | $\mu$V | TIME | $\mu$V | TIME | $\mu$V | TIME | $\mu$V |
| 0 | 6 | 0 | 15 | 0 | 40 | 0 | 2 | 0 | 35 | 0 | 4 |
| 1 | 17 | 1 | 25 | 1 | 44 | 1 | 7 | 1 | 44 | 1 | 12 |
| 2 | 29 | 2 | 34 | 2 | 53 | 2 | 13 | 2 | 54 | 2 | 20 |
| 3 | 39 | 3 | 44 | 3 | 60 | 3 | 20 | 3 | 64 | 3 | 29 |
| 4 | 48 | 4 | 50 | 4 | 66 | 4 | 26 | 4 | 70 | 4 | 39 |
| 5 | 55 | 5 | 58 | 5 | 72 | 5 | 31 | 5 | 80 | 5 | 49 |
| | | | | 6 | 79 | 6 | 38 | | | | |
| 1 | 49 | 1 | 53 | | | | | 1 | 74 | 1 | 48 |
| 2 | 41 | 2 | 45 | 1 | 72 | 1 | 34 | 2 | 62 | 2 | 43 |
| 3 | 34 | 3 | 40 | 2 | 65 | 2 | 27 | 3 | 51 | 3 | 38 |
| 4 | 27 | 4 | 34 | 3 | 57 | 3 | 20 | 4 | 42 | 4 | 34 |
| 5 | 20 | 5 | 28 | 4 | 50 | 4 | 14 | 5 | 35 | 5 | 30 |
| | | | | 5 | 42 | 5 | 8 | | | 6 | 26 |
| | | | | 6 | 34 | | | | | | |

TABLE VII-3. RESULTS OF TESTS

| TEST | 1 | 2 | 3 | 4 | 5 | 6 |
|---|---|---|---|---|---|---|
| Per cent of input power transferred to copper block | 88 | 73 | 65 | 53 | 94 | 52 |

1. TEST CONFIGURATIONS

1. Tight fit of block on diode; diode leads on standoffs.

2. Tight fit of block on diode; diode leads on standoffs; heavy metal clips on diode leads.

3. Large hole in block with block supported by diode; diode leads on standoffs.

4. Large hole in block; block supported so that block does not touch diode; diode leads on standoffs.

5. Large hole in block; space between diode and copper filled with silicone grease; diode leads on standoffs.

6. Test 6 was the same geometrical relationship as Test 5; the diode was mounted in the copper block with high temperature silicone grease; after Test 5 was completed, the block and diode with the silicone grease were baked at 200°C for 30 days before Test 6 was conducted.

2. DISCUSSION:

The principal purpose of this test was to provide data for aid in interpreting the Advent Phase I, II and III tests. For these tests glass bodied diodes were mounted inside a cylindrical cavity bored in an aluminum block and the cavity filled with a high temperature resistant silicone grease. The calculated results in Table VII-3 show that drying of the grease as a result of elevated temperature exposure reduces the heat transferred from the diode body to the block from 94 percent of the total heat initially to 52 percent after one months exposure to 200°C.

The use of the copper block as a calorimeter for the diode body has several limitations. First, is the uncontrolled heat loss from the block. Correction for this was made by determining the rate of cooling of the block after power was removed from the diode. Second, and the one felt to be the largest uncorrected one, is convective heat loss from the diode. In Tests 3 and 4, and to a lesser extent in all the tests, the calculated value is the heat gained by the copper block, not that dissipated through the diode glass body. For all tests except those with the large unfilled hole (Tests 3 and 4) the efficiency of the copper block in absorbing the dissipated heat is probably near unity and somewhat less than unity for Tests 3 and 4. The smallest errors result from neglecting the mass of the diodes in the calculation (0.2gm), the mass of the silicone grease ( $< .01$ gm), and the heating of the copper block by convective heat transfer from the leads.

Sample Calculation: Test 1

Temperature rise of copper block with diode under power (based on data in Table VII-2)

$$\begin{array}{r} 55\ \mu V \\ -6\ \mu V \\ \hline 49\ \mu V \end{array}$$

$49\ \mu V = 9.8$ ($\mu$ V/min.) temperature rise (average)

Cooling of copper block after power was turned off

$$\begin{array}{r} 55 \\ -\ 20 \\ \hline \end{array}$$

$$\frac{35\ \mu V}{5\ \text{min.}} = 7\ \mu\ \text{V/minute (average).}$$

For the small temperature change, the heat loss per unit time on cooling may be used as the heat loss from the block per unit time during heating. Adding this correction to the temperature rise gives

$$\begin{array}{l} 9.8\ \mu V \\ +\ 7\ \ \ \mu V \\ \hline 16.8\ (\mu\ \text{V/min) temperature rise for the copper block} \end{array}$$

$$\frac{16.8\ \mu\ \text{V/min.}}{40\ \ \mu\ \text{V/deg C}} = 0.42\ \text{(degC/min.)}$$ when the $\mu$ V thermocouple reading is converted to temperature.

$$\frac{0.42\ C}{\text{min.}} \times 52.6g \times \frac{.0912\ \text{cal}}{\text{gm degC}} \times \frac{60\ \text{min}}{\text{hour}} \times \frac{.00116\ \text{watt hours}}{\text{cal}} =$$

0.142 watts dissipated to copper block

$$\frac{0.142\ \text{watts into copper} \times 10}{0.154\ \text{watts power dissipated in diode}} =$$ 92% of the dissipated power transferred to copper block.

A correction has to be made for the fact that the heat loss during the cooling period included that from the block back through the diode body and out the leads. Only the heat path from block to air was active during the heating period.

The corrected heat loss is

$7\ \mu$ V/minute x 0.92 = $6.4\ \mu$ V/minute dissipated from block to air.

$$\begin{array}{r} 9.8\ \mu V \\ +\ 6.4\ \mu V \\ \hline 16.2\ \mu V \end{array}$$

and proceeding as before

$$\frac{16.2}{40} \times 52.6 \times 0.0912 \times 60 \times 0.00116 = 0.136\ \text{watts}$$

$$\frac{0.136}{0.154} \times 100 = 88\%$$ of heat dissipated to block.

UNCLAS
Security Classification

**DOCUMENT CONTROL DATA - R&D**

(Security classification of title, body of abstract and indexing annotation must be entered when the overall report is classified)

| 1 ORIGINATING ACTIVITY (Corporate author) | 2a REPORT SECURITY CLASSIFICATION |
|---|---|
| General Electric Co<br>Spacecraft Department, Valley Forge Space Tech Cen<br>King of Prussia, Penn | UNCLAS |
| | 2b GROUP |

3 REPORT TITLE

Accelerated Testing of High Reliability Parts

4 DESCRIPTIVE NOTES (Type of report and inclusive dates)

Interim Technical Documentary Report

5 AUTHOR(S) (Last name, first name, initial)

Walsh, T.
Endicott, H. S.
Best, G.
Bretts, G.
Lampert, H.
Maclean, H.

| 6 REPORT DATE | 7a TOTAL NO OF PAGES | 7b NO OF REFS |
|---|---|---|
| January 1965 | 101 | None |

| 8a CONTRACT OR GRANT NO. | 9a ORIGINATOR'S REPORT NUMBER(S) |
|---|---|
| AF30(602)-3415 | None assigned |
| b. PROJECT NO 5519 | |
| c Task 551902 | 9b OTHER REPORT NO(S) (Any other numbers that may be assigned this report) RADC TDR-64-481 |
| d | |

10 AVAILABILITY/LIMITATION NOTICES

Qualified requesters may obtain copies of this report from DDC.
Release to OTS is authorized - (price unknown)

| 11. SUPPLEMENTARY NOTES | 12. SPONSORING MILITARY ACTIVITY |
|---|---|
| | Reliability Branch<br>Engineering Division<br>Rome Air Development Center, GAFB, NY |

13 ABSTRACT

A review of data and information gathered during previously conducted accelerated test programs has led to the formulation of degradation models for the parts under study. Long term constant stress tests, which were inactive for a 9-month period after accumulating 5000 to 9000 hours of test time at various stress conditions, were restarted. The effect of the passive period on the long-term part parameter trends is discussed. Accelerated step stress test designs and analysis plans were formulated for metal film resistors and semiconductors and step-stress tests were initiated. Failure Mechanism Studies led to the formulation of a current conduction model for glass dielectric capacitors; the detection, possible source and estimated effects of phosphorous compounds on surface leakage of transistors; and low temperature characterization of diode surface leakage currents.

This is an interim report containing information on the first four months of Contract AF30(602)-3415.

DD FORM 1 JAN 64 1473

Security Classification

Security Classification

| 14. KEY WORDS | LINK A | | LINK B | | LINK C | |
|---|---|---|---|---|---|---|
| | ROLE | WT | ROLE | WT | ROLE | WT |
| Accelerated Testing<br>Step-Stress<br>Failure Mechanisms<br>Degradation Models | | | | | | |

INSTRUCTIONS

1. ORIGINATING ACTIVITY: Enter the name and address of the contractor, subcontractor, grantee, Department of Defense activity or other organization *(corporate author)* issuing the report.

2a. REPORT SECURITY CLASSIFICATION: Enter the overall security classification of the report. Indicate whether "Restricted Data" is included. Marking is to be in accordance with appropriate security regulations.

2b. GROUP: Automatic downgrading is specified in DoD Directive 5200.10 and Armed Forces Industrial Manual. Enter the group number. Also, when applicable, show that optional markings have been used for Group 3 and Group 4 as authorized.

3. REPORT TITLE: Enter the complete report title in all capital letters. Titles in all cases should be unclassified. If a meaningful title cannot be selected without classification, show title classification in all capitals in parenthesis immediately following the title.

4. DESCRIPTIVE NOTES: If appropriate, enter the type of report, e.g., interim, progress, summary, annual, or final. Give the inclusive dates when a specific reporting period is covered.

5. AUTHOR(S): Enter the name(s) of author(s) as shown on or in the report. Enter last name, first name, middle initial. If military, show rank and branch of service. The name of the principal author is an absolute minimum requirement.

6. REPORT DATE: Enter the date of the report as day, month, year; or month, year. If more than one date appears on the report, use date of publication.

7a. TOTAL NUMBER OF PAGES: The total page count should follow normal pagination procedures, i.e., enter the number of pages containing information.

7b. NUMBER OF REFERENCES: Enter the total number of references cited in the report.

8a. CONTRACT OR GRANT NUMBER: If appropriate, enter the applicable number of the contract or grant under which the report was written.

8b, 8c, & 8d. PROJECT NUMBER: Enter the appropriate military department identification, such as project number, subproject number, system numbers, task number, etc.

9a. ORIGINATOR'S REPORT NUMBER(S): Enter the official report number by which the document will be identified and controlled by the originating activity. This number must be unique to this report.

9b. OTHER REPORT NUMBER(S): If the report has been assigned any other report numbers *(either by the originator or by the sponsor)*, also enter this number(s).

10. AVAILABILITY/LIMITATION NOTICES: Enter any limitations on further dissemination of the report, other than those imposed by security classification, using standard statements such as:

(1) "Qualified requesters may obtain copies of this report from DDC."

(2) "Foreign announcement and dissemination of this report by DDC is not authorized."

(3) "U. S. Government agencies may obtain copies of this report directly from DDC. Other qualified DDC users shall request through ________________."

(4) "U. S. military agencies may obtain copies of this report directly from DDC. Other qualified users shall request through ________________."

(5) "All distribution of this report is controlled. Qualified DDC users shall request through ________________."

If the report has been furnished to the Office of Technical Services, Department of Commerce, for sale to the public, indicate this fact and enter the price, if known.

11. SUPPLEMENTARY NOTES: Use for additional explanatory notes.

12. SPONSORING MILITARY ACTIVITY: Enter the name of the departmental project office or laboratory sponsoring *(paying for)* the research and development. Include address.

13. ABSTRACT: Enter an abstract giving a brief and factual summary of the document indicative of the report, even though it may also appear elsewhere in the body of the technical report. If additional space is required, a continuation sheet shall be attached.

It is highly desirable that the abstract of classified reports be unclassified. Each paragraph of the abstract shall end with an indication of the military security classification of the information in the paragraph, represented as *(TS)*, *(S)*, *(C)*, or *(U)*.

There is no limitation on the length of the abstract. However, the suggested length is from 150 to 225 words.

14. KEY WORDS: Key words are technically meaningful terms or short phrases that characterize a report and may be used as index entries for cataloging the report. Key words must be selected so that no security classification is required. Identifiers, such as equipment model designation, trade name, military project code name, geographic location, may be used as key words but will be followed by an indication of technical context. The assignment of links, rules, and weights is optional.

Security Classification

BLANK PAGE